AD-A253 897

THE MEAN AND VARIANCE OF DIFFUSE SCATTERED POWER AS A FUNCTION OF CLUTTER RESOLUTION CELL SIZE

Robert J. Papa and Margaret B. Woodworth (ARCON Corp)
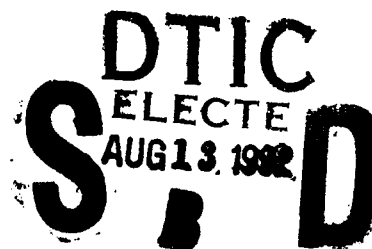
DTIC
ELECTE
AUG 1 3 1992
S D

92 8 10 037

92-22569

This report has been reviewed by the Rome Laboratory Public Affairs Division (PA) and is releasable to the National Technical Information Service (NTIS). At NTIS it will be releasable to the general public, including foreign nations.

RL-TR-91-9 has been reviewed and is approved for publication.

APPROVED:

RAYMOND CORMIER
Acting Chief, Applied Electromagnetics Division
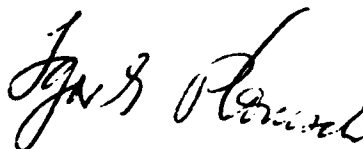Directorate of Electromagnetics

APPROVED:

JOHN K. SCHINDLER
Director of Electromagnetics

FOR THE COMMANDER:

IGOR G. PLONISCH
Directorate of Plans & Programs

If your address has changed or if you wish to be removed from the Rome Laboratory mailing list, or if the addressee is no longer employed by your organization, please notify Rome Laboratory (EECE) Hanscom AFB MA 01731-5000. This will assist us in maintaining a current mailing list.

Do not return copies of this report unless contractual obligations or notices on a specific document require that it be returned.

REPORT DOCUMENTATION PAGE

Public reporting for this collection of information is estimated to average 1 hour per response, including the time for reviewing instructions, searching existing data sources, gathering and maintaining the data needed, and completing and reviewing the collection of information. Send comments regarding this burden estimate or any other aspect of this collection of information, including suggestions for reducing this burden, to Washington Headquarters Services, Directorate for Information Operations and Reports, 1215 Jefferson Davis Highway, Suite 1204, Arlington, VA 22202-4302, and to the Office of Management and Budget, Paperwork Reduction Project (0704-0188), Washington, DC 20503.

1. AGENCY USE ONLY (Leave blank)	2. REPORT DATE	3. REPORT TYPE AND DATES COVERED
	February 1991	In-House 1 Jan 90 - 30 Sep 90

4. TITLE AND SUBTITLE

The Mean and Variance of Diffuse Scattered Power as a Function of Clutter Resolution Cell Size

5. FUNDING NUMBERS

PE 61102F
PROJ 2305
TASK 2305J4
~~JON~~ 2305J409

6. AUTHOR(S)

Robert J. Papa
Margaret B. Woodworth*

7. PERFORMING ORGANIZATION NAME(S) AND ADDRESS(ES)

Rome Laboratory (EEC)
Hanscom AFB, MA 01731-5000

8. PERFORMING ORGANIZATION REPORT NUMBER

RL-TR-91-9

9. SPONSORING/MONITORING AGENCY NAME(S) AND ADDRESS(ES)

10. SPONSORING/MONITORING AGENCY REPORT NUMBER

11. SUPPLEMENTARY NOTES

*Arcon Corp, 260 Bear Hill Road, Waltham, MA 02154-1080

12a. DISTRIBUTION/AVAILABILITY STATEMENT

APPROVED FOR PUBLIC RELEASE; DISTRIBUTION UNLIMITED

12b. DISTRIBUTION CODE

13. ABSTRACT (Maximum 200 words)

In this report, a study is made of the mean and variance of the scattered power as the cell size is varied. These results are based upon a one-dimensional physical optics model for rough surface scattering. The behavior of the mean normalized cross section and the normalized variance is investigated as a function of scattering angle. Parametric studies show the dependence of the statistics on angle of incidence, cell size, rms surface slope, EM wavelength and surface dielectric constant. As the cell size is reduced, the statistical distribution of the scattered power becomes non-Rayleigh. This is more pronounced in the backscatter direction, compared with the forward scattered diffuse power. Also, for small cell sizes, the distribution of the scattered power becomes more non-Rayleigh as the surface roughness is increased.

14. SUBJECT TERMS

Impulse radar
Radar clutter

15. NUMBER OF PAGES

48

16. PRICE CODE

17. SECURITY CLASSIFICATION OF REPORT	18. SECURITY CLASSIFICATION OF THIS PAGE	19. SECURITY CLASSIFICATION OF ABSTRACT	20. LIMITATION OF ABSTRACT
Unclassified	Unclassified	Unclassified	SAR

NSN 7540-01-280-5500

Standard Form 298 (rev. 2-89)
Prescribed by ANSI Std Z39-18
298-102

Preface

This report represents the combined efforts of the authors' individual investigations. Dr. Papa formulated the theory and analyzed the results (Sections 1, 2 and 4). Mrs. Woodworth developed the mathematical techniques (Section 3) and programmed the equations to obtain the numerical results (Section 4). The summary and conclusions (Section 5) were the result of both authors' efforts.

Accession For		
NTIS GRA&I	☑	
DTIC TAB	☐	
Unannounced	☐	
Justification		
By		
Distribution/		
Availability Codes		
Dist	Avail and/or Special	
A-1		

Contents

Illustrations

The Mean and Variance of Diffuse Scattered Power as a Function of Clutter Resolution Cell Size

1. INTRODUCTION

In general, analyses of the statistical properties of EM signals scattered from random rough surfaces have assumed that the surface contributing to the scattering is infinite compared to the characteristic dimension of the roughness (in particular, the correlation length T). Further, the surface is assumed to be homogeneous and isotropic. The result of these assumptions is that the scattered signal tends to have a Rayleigh distribution. The mean scattered power is the product of the mean power per unit area and the area of the cell. If the area is reduced by shrinking the range extent of the cell (corresponding to shorter signal pulses) then the mean clutter power scattered from the surface is reduced so long as the statistical distribution remains unchanged. This report addresses this phenomenon by examining the effect of finite cell size on the calculated statistical properties. The approach is to analyze the behavior of the normalized mean cross section σ^o and normalized variance σ^{oo} of the power as a function of cell size. In this initial study the surface roughness is assumed to be one-dimensional.

First, the theoretical model will be described, followed by an outline of the numerical techniques used to derive the results. Next, the main part of the report presents the results and analyzes them. The behavior of σ^o and σ^{oo} is shown as a function of scattering angle θ_s. Plots

of σ^o and σ^{oo} vs. θ_s are studied for selected values of angle of incidence θ_i, clutter cell size L, rms surface slope $\sqrt{2}\ \sigma/T$ and EM wavelength (carrier wavelength). The two cases where the surface properties are either a perfect conductor or a lossy dielectric are investigated. The plots of σ^{oo} vs. θ_s compare the actual value of σ^{oo} to the value of σ^{oo} assuming the scattered power is a Rayleigh distribution. In the final section, the results are summarized and conclusions offered.

2. THEORETICAL FORMULATION

The analysis begins by assuming that the frequency of the EM wave is characterized by the carrier frequency ω, and that the corresponding wavelength $\lambda = \frac{2\pi c}{\omega}$ is much smaller than the rough surface correlation length T, that is, $T \gg \lambda$. Then, the wave scattering process may be described by physical optics (PO). Both the correlation length and the surface heights are assumed to be described by Gaussian functions. The rough surface heights vary in one dimension only, $\xi = z\ (x)$. Then, following the development given in a previous report[1], the scattering takes place in the plane of variation $(\phi_s = 0°)$ and there is no shadowing.

The normalized cross section of a rough surface σ^o is proportional to

$$\sigma^o \propto\ < (E_s/E_i) \bullet (E_s/E_i)^* > - <(E_s/E_i)>^2 \tag{1}$$

where $< \bullet >$ denotes an ensemble average over the variables $\xi_1, \xi_2, \mu_1, \mu_2$. Here, E_s is the scattered electric field, E_i is the incident electric field, ξ_1 and ξ_2 are the random surface heights at two points x_1 and x_2 and μ_1 and μ_2 are the random surface slopes at the two points. The most general expression for σ^o for a one-dimensional rough surface involves a six-fold integral over the variables $x_1, x_2, \xi_1, \xi_2, \mu_1,$ and μ_2. By using the fact that the surface heights are to be regarded as a stationary random process, so that the correlation function of the surface heights, $c\ (\tau)$, is a function only of the separation between points $\tau = x_1 - x_2$, the six-fold integral for σ^o may be reduced to a five-fold integral. Then, using the fact that the general expression for σ^o is a function only of the height differences $\xi = \xi_1 - \xi_2$, the five-fold integral can be reduced to a four-fold integral. Making the additional assumption that the rms slope $\sqrt{2}\ \sigma/T < 1$ (where σ = rms surface height) permits the surface heights to be decorrelated from the surface slopes. Then, the integrations over the surface slopes μ_1 and μ_2 may be readily performed, so that the expression for σ^o for a finite clutter cell reduces to a double integration. Under these same assumptions, and using the expression for the scattered electric field based upon physical optics (PO), an expression for the normalized variance of the power σ^{oo} may be

---

[1] Papa, R.J., and Woodworth, M. (1988) *The Numerical Evaluation of a Physics Optics Normalized Cross Section for a Rough Surface*, RADC-TR-87-280, ADA198919.

2

derived. For a clutter cell of finite size, the normalized variance σ^{oo} may be expressed as a four-fold integral.

Since the surface is assumed to be rough in one dimension only, the scattered field is a cylindrical wave

$$E_s = \sqrt{2/\left(\pi \mathbf{k}_s \cdot \mathbf{R}'\right)} \, \exp\left[i\,\mathbf{k}_i \cdot \mathbf{R}'\right] \tag{2}$$

where $\mathbf{k}_s$ = scattered wave number

$$\mathbf{R}' = \mathbf{R}_o - \mathbf{r}$$
$$\mathbf{R}_o = \text{distance from origin to field point}$$
$$\mathbf{r} = \text{distance from origin to source on the surface.}$$

The scattered field is calculated by evaluating the Helmholtz integral (Beckmann and Spizzichino[2]):

$$E_s = \frac{1}{4\pi} \int_L \left(E \frac{\partial \psi}{\partial n} - \psi \frac{\partial E}{\partial n} \right) dx \tag{3}$$

where

$$\psi = \sqrt{2/\left(\pi \mathbf{k}_s \cdot \mathbf{R}'\right)} \, \exp\left[i\,\mathbf{k}_s \cdot \mathbf{R}'\right] \tag{4}$$

$\dfrac{\partial}{\partial n}$ = normal derivative on the surface S. (Here, we integrate over only one dimension, x).

[2] Beckmann, P., and Spizzichino, A. (1987) *The Scattering of Electromagnetic Waves from Rough Surfaces*, Artech House, Inc., Dedham, MA.

It is assumed, under the PO approximation, that the total field on S is given by

$$E = (1 + R) E_i \qquad (5)$$

where

R = Fresnel plane wave reflection coefficient.

By combining Eqs. (2), (3), (4), and (5) and using the assumptions given in the previous discussions, an expression for the scattered wave may be obtained (see Beckmann and Spizzichino[2]):

$$E_s = \left(\frac{i\,e^{(ikR_0)}}{4\pi} \right) \left(\sqrt{\frac{2}{\pi k R_o}} \right) F \int_{-L/2}^{L/2} \exp\left[i\,\mathbf{v} \cdot \mathbf{r}\right] dx \qquad (6)$$

where

$$\mathbf{v} = k\left[\left(\sin\theta_i - \sin\theta_s\right) \hat{x} - \left(\cos\theta_i + \cos\theta_s\right) \hat{z} \right]$$

$$= v_x\,\hat{x} + v_z\,\hat{z}$$

and $\quad k = 2\,\pi/\lambda.$

Here,

$$F = \left[2R\left(1 + \cos\left(\theta_i + \theta_s\right)\right) / \left(\cos\theta_i + \cos\theta_s\right) \right] \qquad (7)$$

and we have assumed a horizontally polarized incident wave, and thus we also specify the appropriate form for R.

4

The expression for the normalized cross section σ^o of a one-dimensional rough surface is given by:

$$\sigma^o = (2\,\pi\,R_o/L)\left[<|E_s/E_i|^2> - <|E_s/E_i|>^2\right] \tag{8}$$

where $< \bullet >$ denotes an ensemble average over the surface heights. One may then derive the following expression for σ^o:

$$\sigma^o = \left(\frac{F^2}{2\pi L\,\lambda}\right)\int_{-L/2}^{L/2}dx_1\int_{-L/2}^{L/2}dx_2\left[\chi_2 - \chi_1\chi_1^*\right]\cos v_x\tau \tag{9}$$

where $\tau = x_1 - x_2$

χ_2 = characteristic function for bivariate height distribution
$\quad = \exp\left[-\sum^2(1 - C_{12})\right]$
χ_1 = characteristic function for univariate height distribution
$\quad = \exp\left[-\sum^2/2\right]$
$C_{12} = \exp\left[-(x_1-x_2)^2/T^2\right]$
$\sum^2 = \sigma^2 v_z^2$ = Rayleigh parameter squared.

The normalized variance in clutter power σ^{oo} is defined in terms of the fourth moment of the scattered field:

$$\sigma^{oo} = \left(\frac{2\,\pi\,R_o}{L}\right)^2\left(<|E_s/E_i|^4> - <|E_s/E_i|^2>^2\right). \tag{10}$$

First, consider the term

$$<|E_s/E_i|^2> \propto \int_{-L/2}^{L/2}dx_1\int_{-L/2}^{L/2}dx_2\,e^{iv_x(x_1-x_2)}<e^{iv_z(\xi_1-\xi_2)}> \tag{11}$$

5

$$= \int_{-L/2}^{L/2} dx_1 \int_{-L/2}^{L/2} dx_2 \exp\left[i v_x (x_1 - x_2)\right] \chi_2.$$

Next, consider the square of the second moment of the scattered wave:

$$< |E_s / E_j|^2 > < |E_s / E_j|^2 > \tag{12}$$

$$\propto \int_{-L/2}^{L/2} dx_1 \int_{-L/2}^{L/2} dx_2 \int_{-L/2}^{L/2} dx_3 \int_{-L/2}^{L/2} dx_4 \cdot \exp\left[i v_x ((x_1 - x_2) + (x_3 - x_4))\right]$$

$$\cdot \exp\left[-v_z^2 \sigma^2 \left[(1 - C_{12}) + (1 - C_{34})\right]\right]$$

where $C_{ij} = \exp\left[-(x_i - x_j)^2 / T^2\right]$.

The ensemble average of the fourth moment of the scattered electric field is given by

$$< |E_s / E_j|^4 > \propto \int_{-L/2}^{L/2} dx_1 \int_{-L/2}^{L/2} dx_2 \int_{-L/2}^{L/2} dx_3 \int_{-L/2}^{L/2} dx_4 \, e^{i v_x (x_1 - x_2 + x_3 - x_4)} \tag{13}$$

$$\cdot < e^{i v_z (\xi_1 - \xi_2 + \xi_3 - \xi_4)} >$$

Define the fourth order characteristic function χ_4 as

$$\chi_4 = < e^{i v_z (\xi_1 - \xi_2 + \xi_3 - \xi_4)} > \tag{14}$$

6

$$= \int_{-\infty}^{\infty} d\xi_1 \int_{-\infty}^{\infty} d\xi_2 \int_{-\infty}^{\infty} d\xi_3 \int_{-\infty}^{\infty} d\xi_4 \left[e^{iv_z \left(\xi_1 - \xi_2 + \xi_3 - \xi_4 \right)} \right] P \left(\xi_1, \xi_2, \xi_3, \xi_4 \right)$$

where $P \left(\xi_1, \xi_2, \xi_3, \xi_4 \right)$ is the fourth order height distribution function. For a Gaussian distribution,

$$P \left(\xi_1, \xi_2, \xi_3, \xi_4 \right) = \left((2\pi)^2 [\mathrm{DET}\ C]^{1/2} \right)^{-1} \exp \left[- (1/2)\ \xi^T\ C^{-1}\ \xi \right] \tag{15}$$

where

$$\xi = \begin{bmatrix} \xi_1 \\ -\xi_2 \\ \xi_3 \\ -\xi_4 \end{bmatrix}$$

and the covariance matrix C is given by

$$C = \sigma^2 \begin{bmatrix} 1 & C_{12} & C_{13} & C_{14} \\ C_{21} & 1 & C_{23} & C_{24} \\ C_{31} & C_{32} & 1 & C_{34} \\ C_{41} & C_{42} & C_{43} & 1 \end{bmatrix}.$$

It is known that the Fourier transform of a Gaussian is also a Gaussian (Stark and Woods[3]):

$$\chi_4 = \exp \left[- (1/2)\ \omega^T\ C\ \omega \right] \tag{16}$$

---

[3] Stark, H., and Woods, J. (1986) *Probability, Random Processes and Estimation Theory for Engineers*, Prentice-Hall, New York.

where

$$\omega = \begin{pmatrix} v_z \\ -v_z \\ v_z \\ -v_z \end{pmatrix}.$$

After some algebraic manipulations, the expression for χ_4 may be derived:

$$\chi_4 = \exp\left[-\Sigma^2 \left(2 - C_{12} + C_{13} - C_{14} - C_{23} + C_{24} - C_{34}\right)\right]. \tag{17}$$

Then, combining Eqs. (10) through (16), one may obtain the following expression for the variance in power

$$\sigma^{\infty} = \left(F^2/[2\pi\lambda L]\right)^2 \int_{-L/2}^{L/2} dx_1 \int_{-L/2}^{L/2} dx_2 \int_{-L/2}^{L/2} dx_3 \int_{-L/2}^{L/2} dx_4 \cos\left[v_x\left(x_1 - x_2 + x_3 - x_4\right)\right] \bullet \left[\chi_4 - \chi_{12}\,\chi_{34}\right]. \tag{18}$$

Here, $\chi_{12} = \exp\left[-\Sigma^2 \left(1 - C_{12}\right)\right]$
and $\chi_{34} = \exp\left[-\Sigma^2 \left(1 - C_{34}\right)\right]$.

If the statistical distribution of the power scattered from a clutter cell is Rayleigh, then

$$\sigma^{o} \propto \overline{P}_s \tag{19}$$

where $\overline{P}_s$ is the mean of the scattered wave. Eq. (19) is true for any statistical distribution. But the variance in the power, for a Rayleigh distribution, is given by:

$$\sigma^{\infty} \propto \overline{P^2}_s - \overline{P}_s^2 = \overline{P}_s^2. \tag{20}$$

Eq. (20) is true only for a Rayleigh distribution. The definitions of σ^o and σ^{∞} given in this report are such that, for a Rayleigh distribution:

$$\sigma^{\infty} = \left(\sigma^{0}\right)^{2}.$$

(21)

3. NUMERICAL METHODS

The four-fold integral in Eq. (18) and the two-fold integral in Eq. (9) must be solved numerically. Any quadruple integral will require many function evaluations. The key is to use an efficient numerical integration algorithm that minimizes the required number of function evaluations. We used three different methods: two Monte Carlo routines and an adaptive Gauss quadrature routine. These three methods have different strengths and weaknesses, thus none is superior to the others in all situations.

The first Monte Carlo routine we used is a modified version of a routine obtained from the Press and Farrar[4] paper, titled "Recursive Startified Sampling for Multidimensional Monte Carlo Integration". The four-dimensional region to be integrated is first sampled to determine the distribution of the function. The region is then divided up into subregions each assigned a certain percentage of the points where the function is evaluated. In this way, the largest number of function evaluations are concentrated where the function is most significant. The points in each four-dimensional subregion are determined by a uniform random number generator. The function is evaluated at these points and the integrand value for each subregion is determined. The overall integral is found by combining all subregions. The standard deviation of the answer is also calculated. If the standard deviation is too large (> 1%), then the number of points is increased up to a maximum of about 7×10^{7}. Beyond this number the round-off error becomes the main factor limiting the accuracy.

The second Monte Carlo routine is based on the Press and Teukolsky[5] paper titled "Quasi- (that is, Sub-) Random Numbers". Simple Monte Carlo integration relies on points distributed at random over the region to be integrated. The fractional error of the estimated integral decreases by $1/\sqrt{N}$, where N is the number of sample points. Press and Teukolsky show that when the multidimensional points are determined by a subrandom Sobol sequence, the fractional error decreases at a rate close to $1/N$. (The points generated by the Sobol sequence appear random when plotted, but actually the Sobol sequence deterministically chooses points in space which maximally avoid each other and fill the space more uniformly than uncorrelated random points.) The integral can be accurately determined with many fewer

[4] Press, W.H., and Farrar, G.R. (1990) Recursive stratified sampling for multidimensional Monte Carlo integration, *Computers in Physics*, 4:190-195, March/April.

[5] Press, W.H., and Teukolsky, S.A. (1989) Quasi- (that is, sub-) random numbers, *Computers in Physics*, 3:76-79, November/December.

function evaluations than the standard Monte Carlo method. The function is evaluated at each point and the values are summed to give the value of the integral. The standard deviation is also determined. If the result is not accurate enough, the Sobol sequence is simply extended until the desired accuracy is reached, up to a limit of 2^{31} points.

The adaptive Gauss quadrature routine is based on an integration routine presented by Shampine and Allen[6] We converted their routine from one based on Simpson's rule to one based on four-point Gauss quadrature. We further modified the routine to solve the multi-dimensional integration, and to improve its efficiency. The basic technique is simple. First an integral is evaluated with four-point Gauss quadrature, then the integral is bisected and each half is evaluated separately with four-point Gauss quadrature and the halves summed. If the two results are different by more than the desired accuracy, then the right half is stored and the left half is again bisected and each new section is evaluated. Again the accuracy is checked by comparing the sum of the evaluations over the two quarters with that of the half interval. Bisection continues until either the desired accuracy is reached or the subsection becomes too small. In either case, the values of the subsections are stored and the routine moves to the next subsection to the right, which is also bisected until the desired accuracy is reached. In order to maintain the given overall accuracy, the accuracy is divided by the square root of 2 with each finer level of bisection. The evaluations over the set of subsections are summed to give the total integrand. This adaptive method concentrates the computational effort where it is most needed and avoids wasting effort where it is not required. This is done for all four levels of integration. In the outer integration, an error threshold is determined which is passed to the inner integrals, if the value of a subsection falls below the threshold, it is marked "done" even if it has not converged, because the value is too small to significantly contribute to the final result.

The three methods are driven by different mechanisms. The number of function evaluations is a user input for our first Monte Carlo method and the error bound of the result is determined from the data. Since the computer CPU time is proportional to the number of evaluations, we know ahead of time how long the first Monte Carlo method will take. Conversely, the error bounds are a user input for the second Monte Carlo method and the adaptive Gauss quadrature, and the function is evaluated as many times as necessary to achieve that accuracy; thus the amount of time can vary widely depending on the exact structure of the function. The first Monte Carlo method is also susceptible to accuracy problems if the function oscillates. The adaptive methods are better able to compensate for any oscillations. The oscillations come primarily from the term cos $(v_x (x_1 - x_2 + x_3 - x_4))$ in Eq. (18). Doubling the length of a cell (L) will double the range of each dimemsion of the integral and thus double the number of oscillations in each dimension. Another factor is $v_x = k (\sin \theta_i - \sin \theta_s)$ which contributes the effect of wavelength and the angle terms. The further apart the incident and scatter angles, the more oscillations. Generally, when v_x is small, any method is accurate, but the Monte Carlo methods are much more efficient, up to orders of magnitude faster than adaptive Gauss quadrature. As the number of oscillations

[6] Shampine, L.F., and Allen, R.C. (1973) *Numerical Computing: An Introduction*, W.B. Saunders Company.

increase, the first Monte Carlo method becomes inaccurate and the second Monte Carlo method and Gauss quadrature become the more accuracte methods of integration. However, the run time of the Gauss quadrature routine also increases dramatically as the oscillations increase. These two factors put a practical limit on the range of scatter angles that can be used with a given data set. The second Monte Carlo method is generally the fastest and most accurate method for the widest range of angles.

The two-fold integral Eq. (9) is evaluated in a similar manner as the four-fold integral [Eq. (18)]. As expected, the two-fold integral can be evaluated much faster than the four-fold integral. Once the integral is found it is a simple matter to convert from σ^o and σ^{oo} for a perfect conductor to σ^o and σ^{oo} for a dielectric surface. Simply use the appropriate value of F in Eqs. (9) and (18).

4. ANALYSIS OF NUMERICAL RESULTS

In this section, a number of graphs will be presented of σ^o vs θ_s and σ^{oo} vs θ_s, with parameters that include the angle of incidence θ_i, wavelength λ, standard deviation in surface height σ, surface correlation length T, length of rough surface L, and complex dielectric constant ε. The curve indicated with long dashed lines represents σ^o as calculated numerically according to Eq. (9). The curve indicated by crosses represents σ^{oo} as calculated numerically according to Eq. (18). The curve indicated by short dashes represents σ^{oo} for a Rayleigh distribution, as given by Eq. (21) with the value of σ^o given by Eq. (19).

In Figures 1 through 24, we will study the behavior of σ^o and σ^{oo} vs scattering angle θ_s for different parameter regimes. First, the angle of incidence θ_i is chosen to be relatively small ($\theta_i = 30^o$) and then, later, is taken to be large ($\theta_i = 75^o$). The wavelength is first taken at L-band ($\lambda = 0.25m$) and then decreased to S-band ($\lambda = 0.1m$). The cell size is first taken to be small (L = 3T), then increased to L = 6T, and eventually to L = 12T. Also, the surface roughness starts out at a relatively small value ($\sigma/T = 0.2$) and then is increased to $\sigma/T = 0.5$.

In Figure 1, the values of the parameters are $\theta_i = 30^o$, $\lambda = 0.25m$, $\sigma = 0.2$, T = 1m, L = 3m, and ε is a perfect conductor. For a large clutter cell (L $\geq$ 10T), the scattered power is Rayleigh distributed (Beckmann and Spizzichino[2]). The comparison of the exact σ^{oo} with the Rayleigh value of σ^{oo} shows that for a short cell size (L = 3T), the clutter power is Rayleigh distributed in an angular region about the specular direction ($\theta_s = \theta_i$), where the angular region extends from about $\theta_s = 50^o$ to 0°. As θ_s moves away from the angular region, the clutter power becomes more non-Rayleigh, and the departure from the Rayleigh distribution is more dramatic in the backscatter region $\theta_s < 0^o$ than in the forward scatter region $\theta_s > 50^o$.

In Figure 2, the parameters are the same as in Figure 1, except that now ε is a complex dielectric (30 + j2), representing moist loam. Although the results will not be shown here, a whole set of complex dielectric constants were investigated, where the parameters were the same as in Figure 1 except that ε = (2 + j4), (2 + j0), (4 + j2), (4 + j0), (80 + j9), and (80 + j0). The results may be summarized by stating that the values of σ^o and σ^{oo} are less for a complex

dielectric surface compared to a perfect conductor, indicating a general trend. Also, it may be stated that, for a complex dielectric surface, increasing either the real or imaginary part of ε causes both σ^o and σ^{oo} to increase. In Figure 3, the parameters are the same as in Figure 1, except that the cell size is larger, with $L = 6T$. Comparing Figure 3 with Figure 1, it may be noted that the larger cell size results in σ^{oo} being closer to the Rayleigh distribution. In Figure 4, the parameters are the same as in Figure 2, except that $L = 6T$. Again, the larger cell size results in σ^{oo} being closer to the Rayleigh value, for the surface with a complex dielectric constant.

In Figures 5 and 6, the parameters are the same as in Figures 1 and 2, except that $\sigma = 0.5m$, so that $\sigma/T = 0.5$ (a rougher surface). Comparing Figures 5 and 6 with Figures 1 and 2, one may note that σ^o is more constant in value (flatter) as θ_s varies, indicating that the rougher surface scatters more isotropically, both for a perfect conductor and a lossy dielectric. Also, σ^{oo} is less close to the Rayleigh value of $(\sigma^o)^2$ as the surface gets rougher, both for a perfect conductor and a lossy dielectric. In Figures 7 and 8, the parameters are the same as in Figures 5 and 6, except that the cell size is larger, $L = 6T$. The increase in cell size causes the true variance σ^{oo} to decrease, becoming closer to the variance for a Rayleigh distribution.

In Figures 9 and 10, the angle of incidence has been changed so that $\theta_i = 75^o$, with all the other parameters equal to those in Figures 1 and 2. Comparing Figures 9 and 10 with Figures 1 and 2, one may note that increasing the angle of incidence results in smaller values of σ^o and σ^{oo}, for both a perfect conductor and a lossy dielectric. Again, it may be noted that the variance σ^{oo} is close to a Rayleigh distribution in an angular region about the specular direction $\theta_s = \theta_i$, and deviates from it as θ_s moves away from this angular region. As in Figures 1 and 2, the departure from the Rayleigh distribution is more dramatic for the backscatter region, $\theta_s < 0^o$ than for the forward scatter region.

In Figures 11 and 12, the parameters are the same as in Figures 9 and 10, except the cell size is larger, $L = 6T$. The increase in cell size results in the variance σ^{oo} values becoming closer to the Rayleigh distribution values, for both a perfect conductor and a lossy dielectric. In Figures 13 and 14, the parameters are the same as in Figures 11 and 12, except that the cell size has been increased further, to $L = 12T$. This further increase results in the σ^{oo} values becoming almost equal to the Rayleigh distribution values.

In Figures 15 and 16, the parameters are the same as in Figures 9 and 10, except that the standard deviation in surface height has been increased, $\sigma = 0.5m$, so that the surface is rougher with $\sigma/T = 0.5$. The increase in surface roughness causes the values of σ^o and σ^{oo} to increase. Also, the vaues of σ^{oo} deviate more pronouncedly from the Rayleigh distribution values. In Figures 17 and 18, the parameters are the same as in Figures 15 and 16, except that the cell size has been increased to $L = 6T$. As shown previously, the increase in cell size causes the σ^{oo} values to be closer to those of a Rayleigh distribution.

In Figures 19 through 24, the EM wavelength has been changed to $\lambda = 0.1m$, so that S-band microwave radiation is being considered, instead of L-band ($\lambda = 0.25m$). The parameters in Figures 19 and 20 are the same as in Figures 1 and 2, except for the EM wavelength. Comparing Figures 19 and 20 with Figures 1 and 2, one may note that the decrease in λ results in a slight reduction in σ^o for $\theta_s < 0^o$. Also, the σ^{oo} values have increased, with a greater deviation from the Rayleigh distribution values.

In Figures 21 and 22, the parameters are the same as in Figures 9 and 10, except that the EM wavelength has been reduced to $\lambda = 0.1$m. Comparing Figures 21 and 22 to Figures 9 and 10, it may be observed that the decrease in λ causes the σ^o values to decrease for $\theta_s < 0^o$. Also, the σ^{oo} values have increased, exhibiting a greater deviation from the Rayleigh distribution values.

In Figures 23 and 24, the parameters are the same as in Figures 21 and 22, except that the cell size has been increased to $L = 6T$. As at L-band, the increase in cell size causes the σ^{oo} values to be closer to the Rayleigh distribution values.
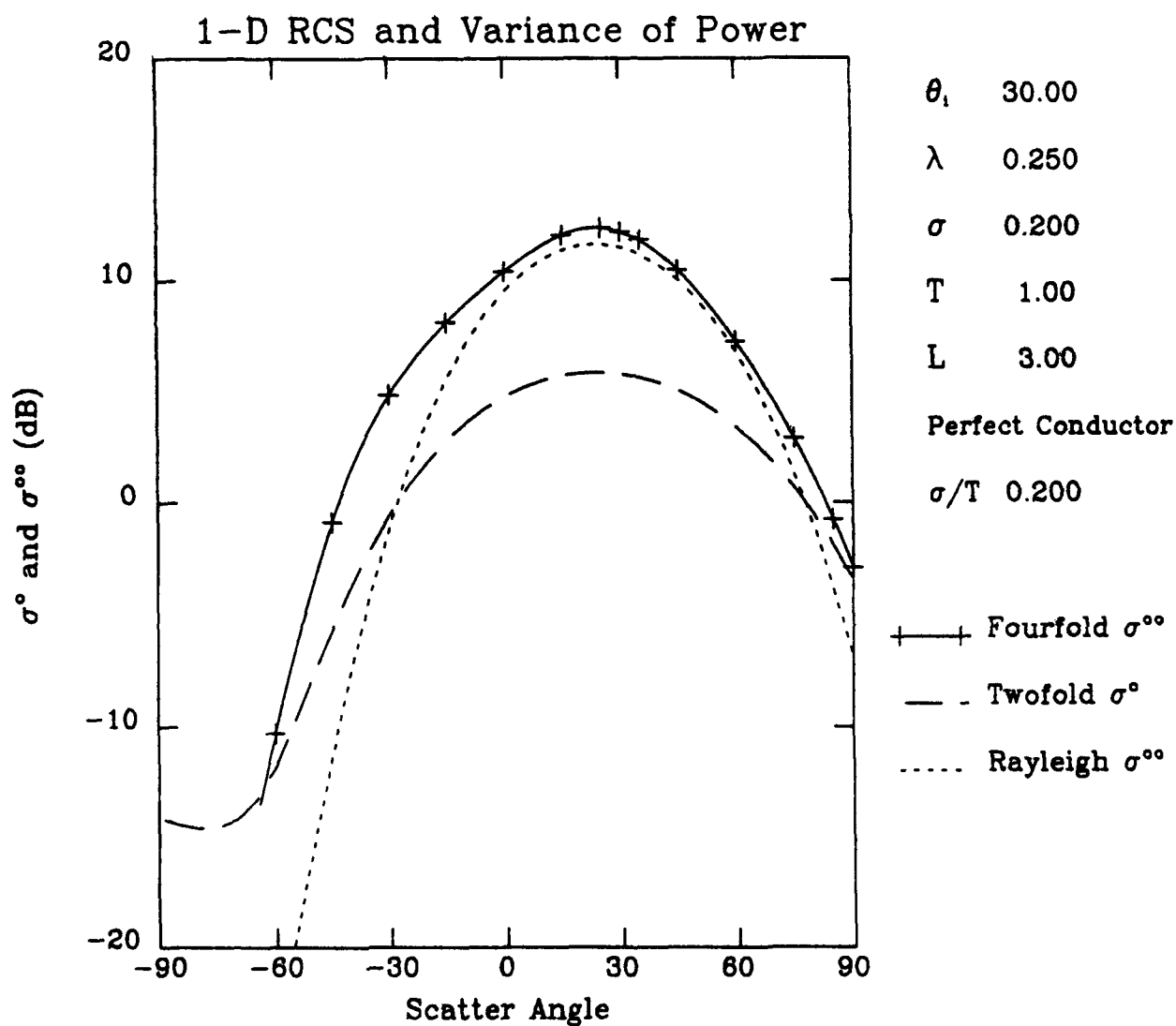
Figure 1. Graph of σ^o and σ^{oo} vs θ_s for a Perfect Conductor, $\theta_i = 30°$, Small Slope, Small Cell.

14
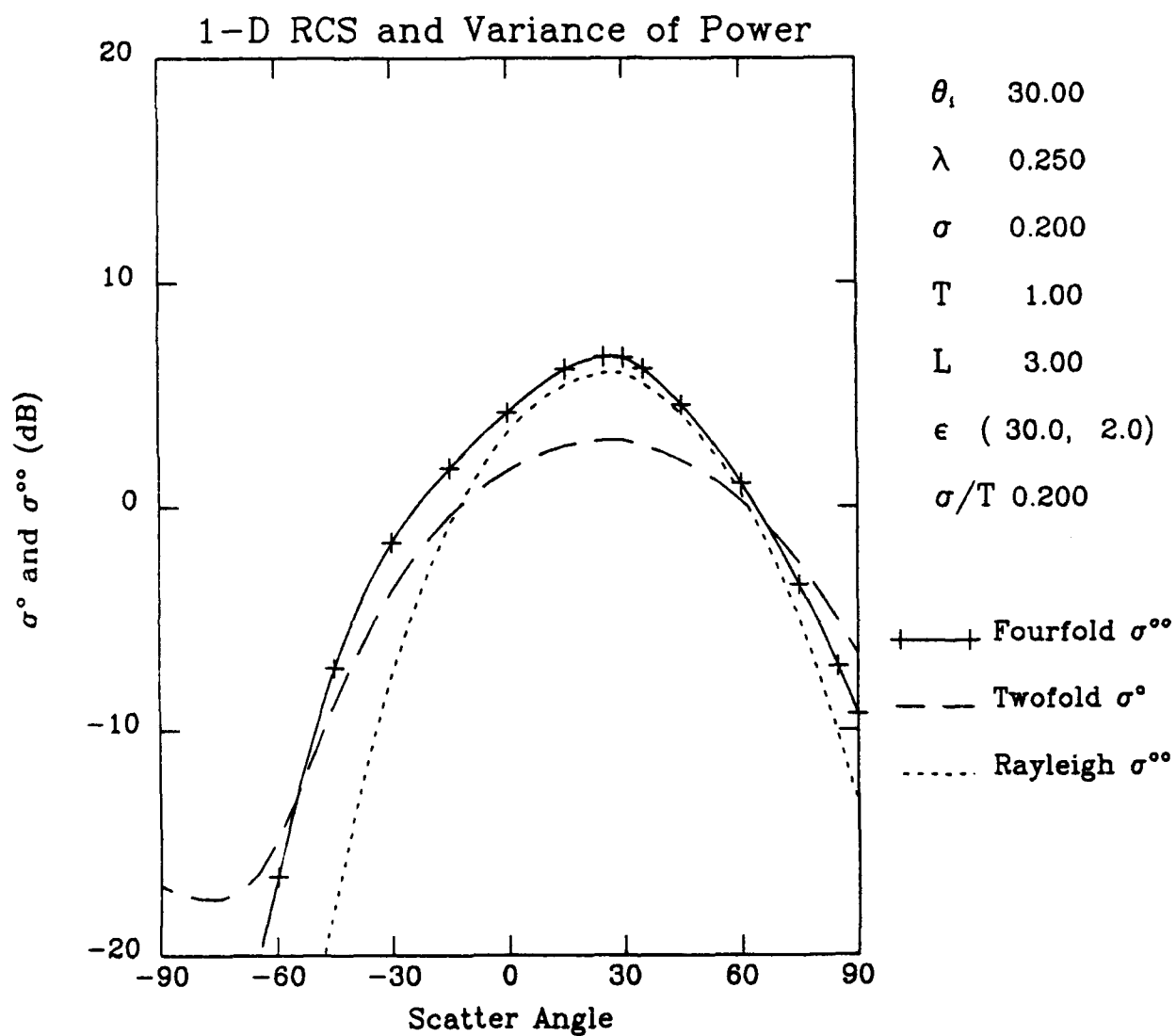
Figure 2. Graph of σ^o and σ^{oo} vs θ_s for a Lossy Dielectric, $\theta_i = 30^\circ$, Small Slope, Small Cell.
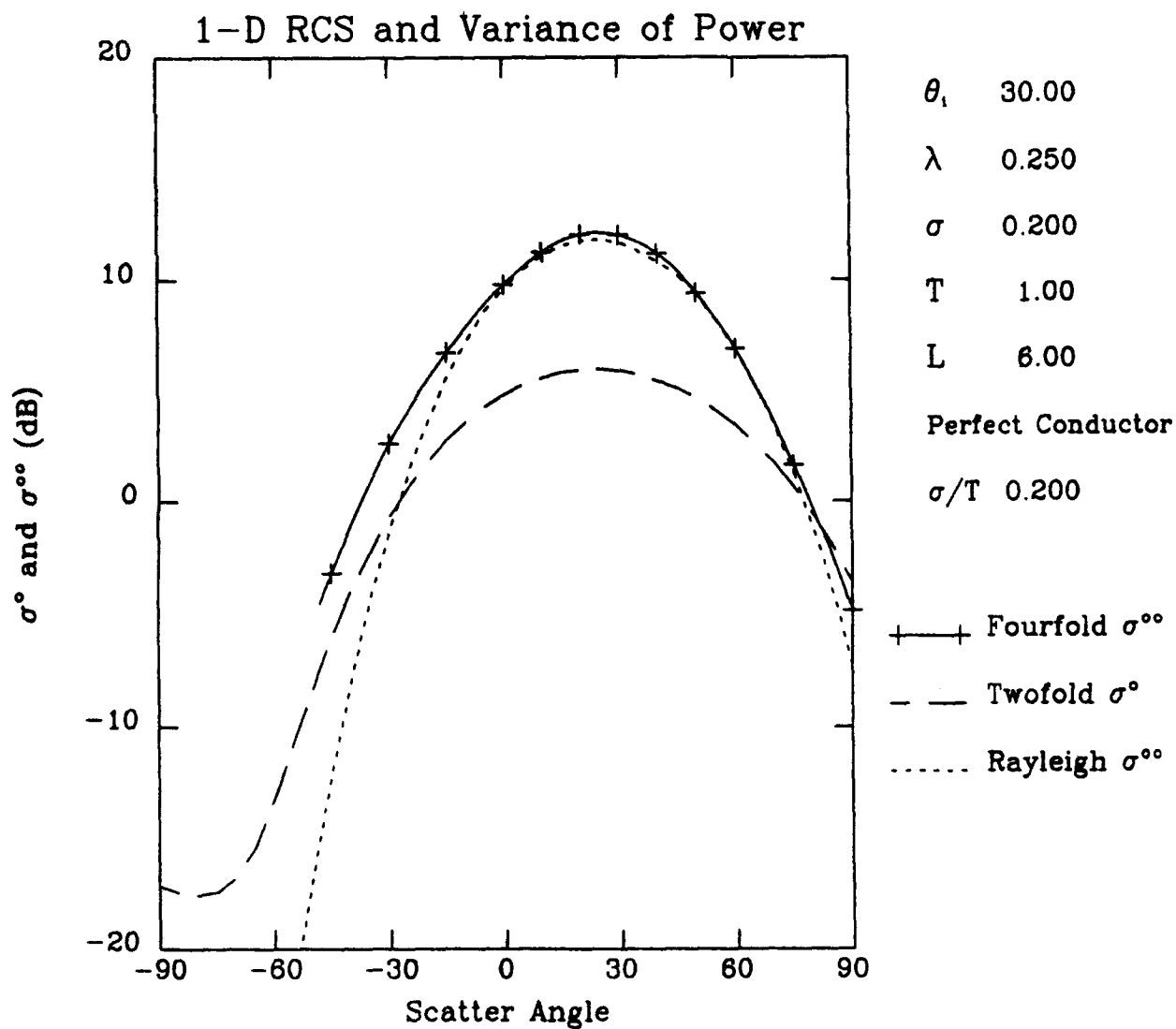
Figure 3. Graph of σ^o and σ^{oo} vs θ_s for a Perfect Conductor, $\theta_i = 30°$, Small Slope, Intermediate Cell.
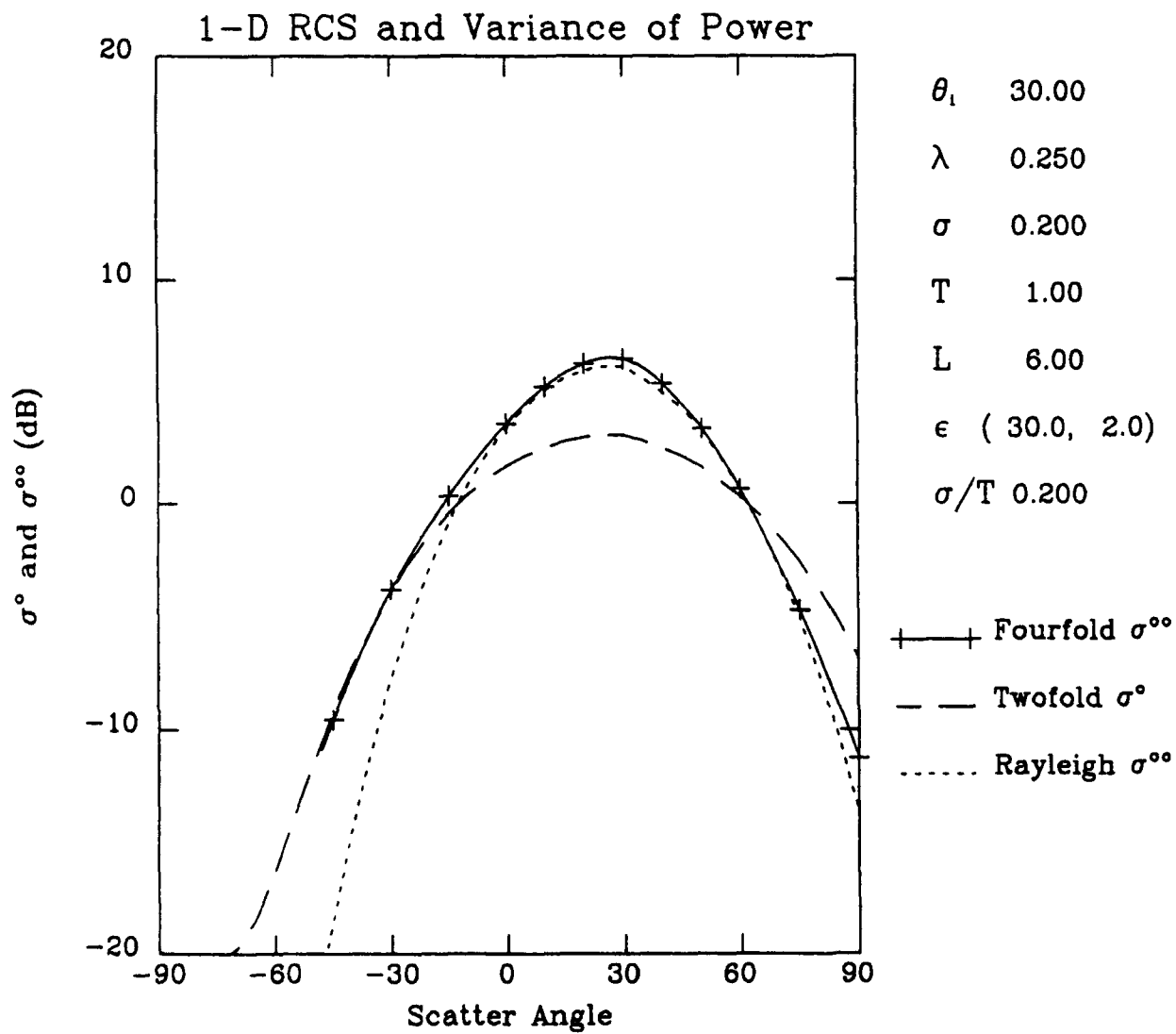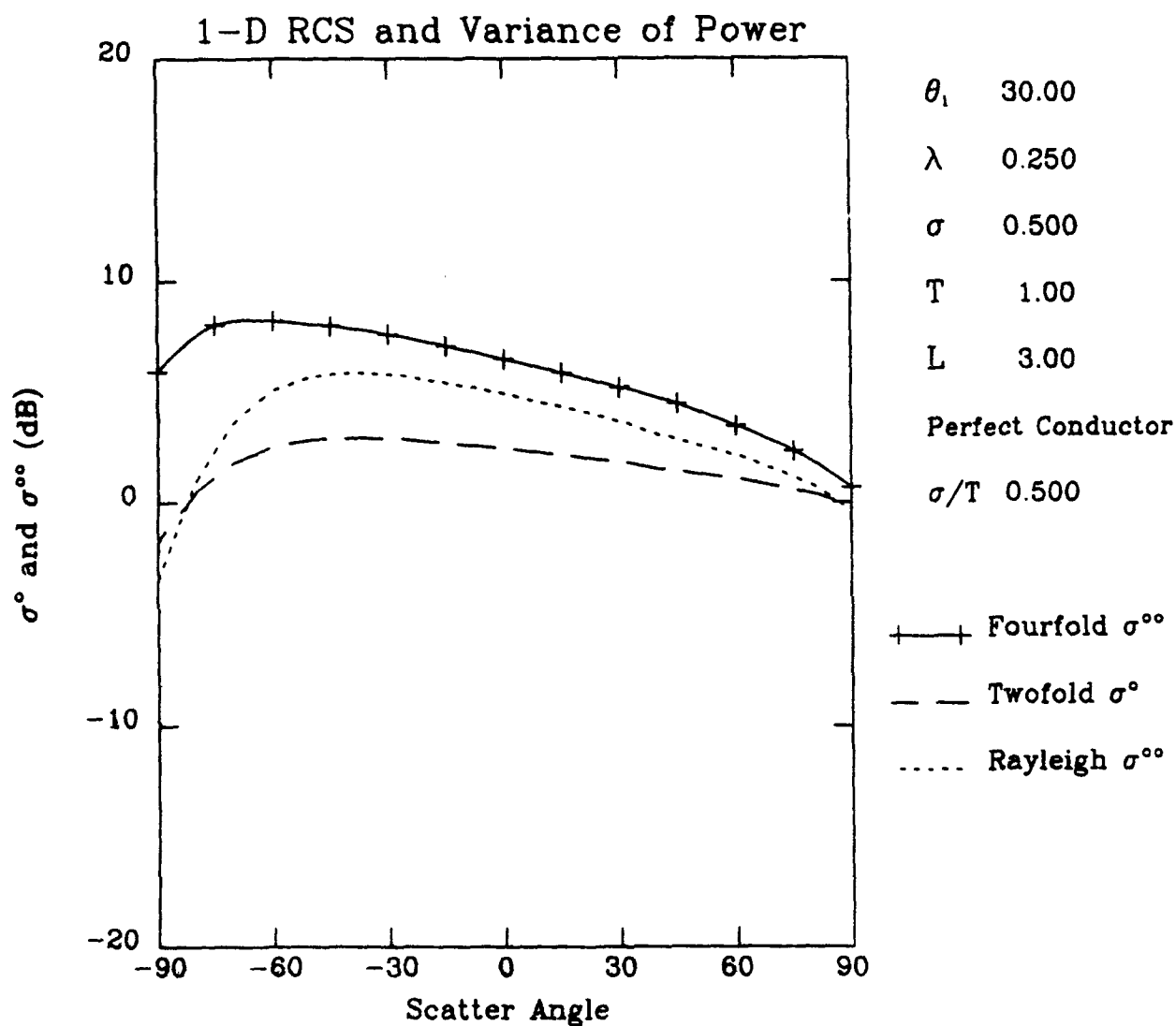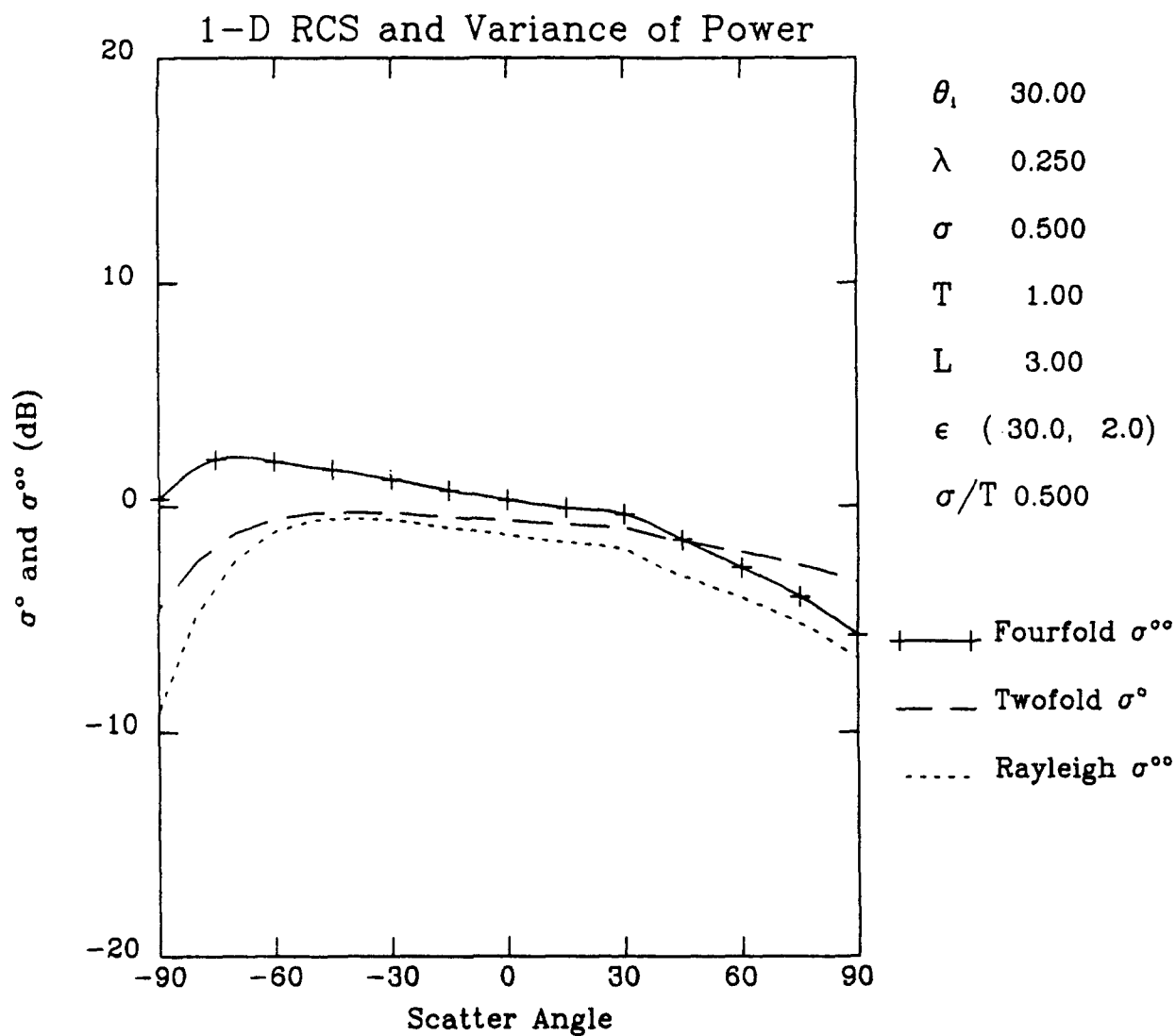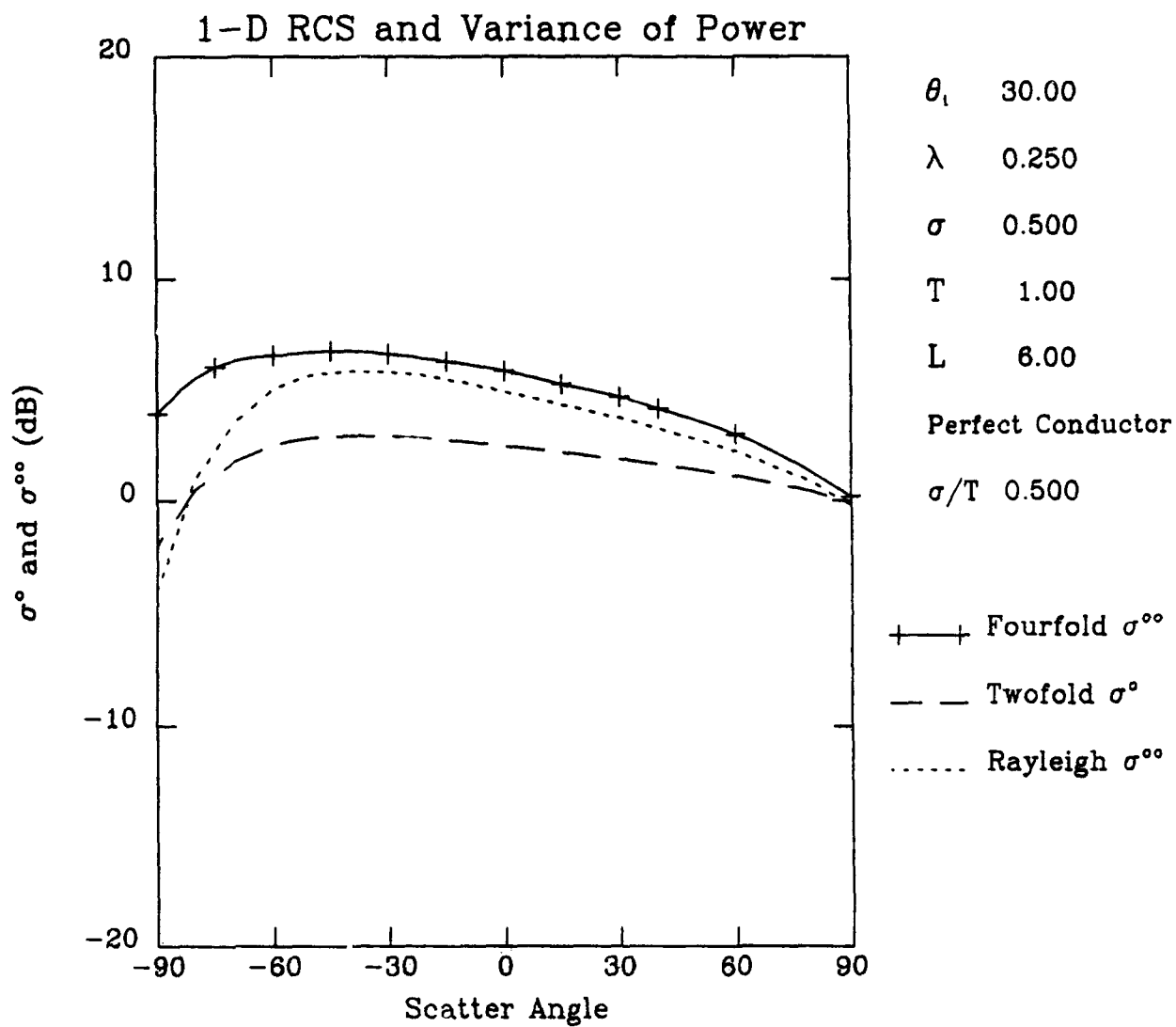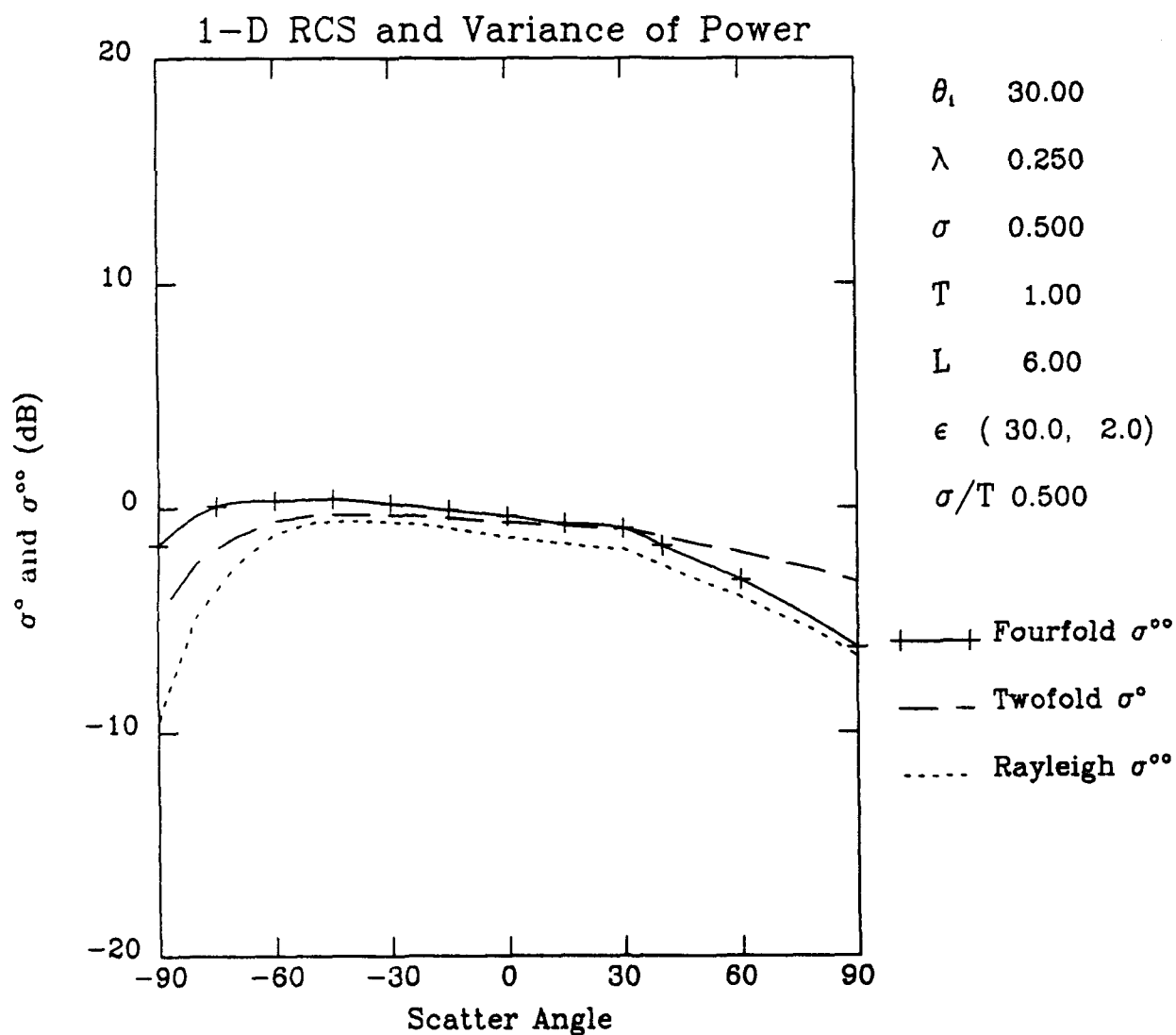
Figure 4. Graph of σ^o and σ^{oo} vs θ_s for a Lossy Dielectric, $\theta_i = 30^o$, Small Slope, Intermediate Cell.
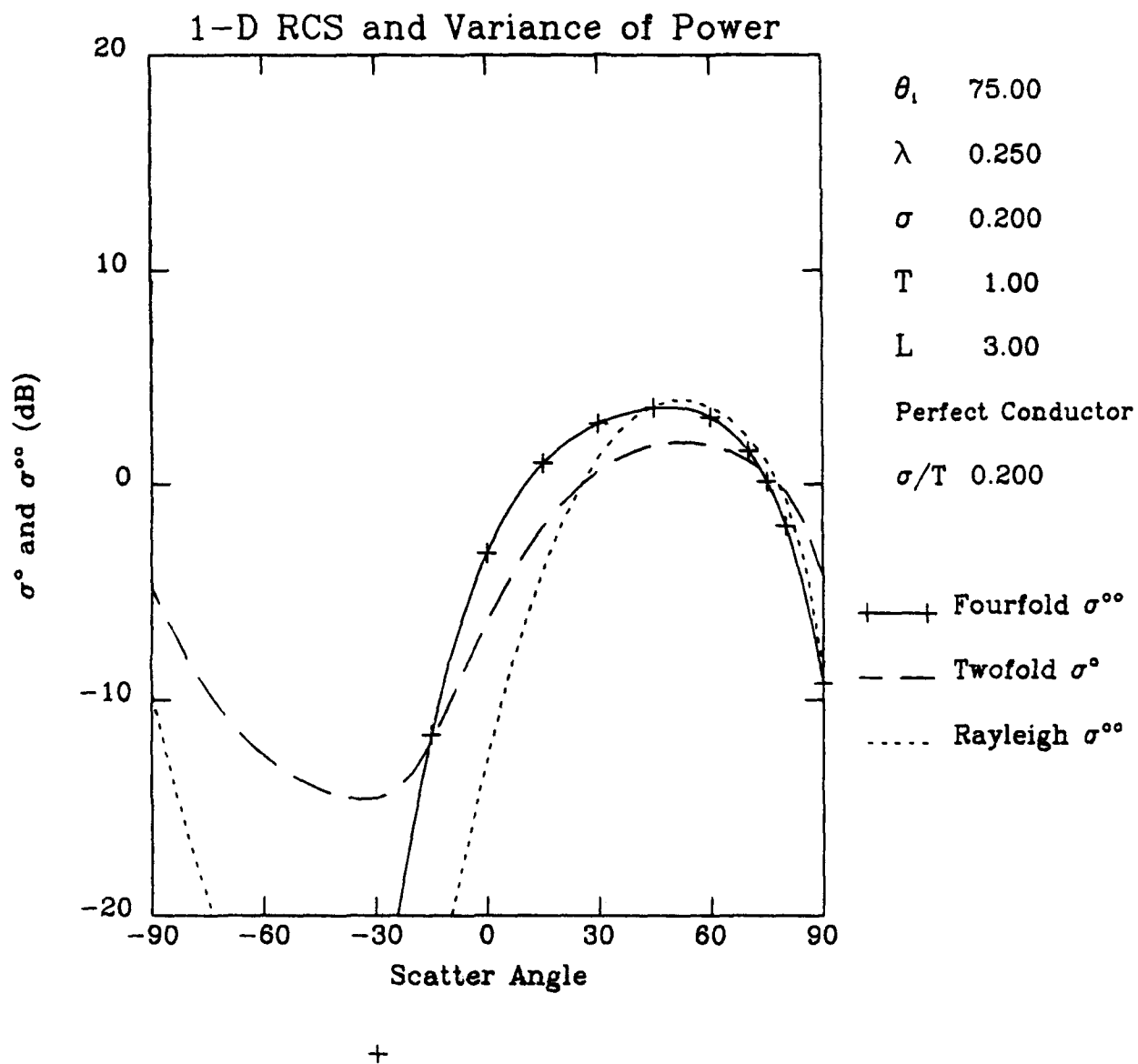
Figure 5. Graph of σ^o and σ^{oo} vs θ_s for a Perfect Conductor. $\theta_i = 30^o$. Large Slope. Small Cell.

Figure 6. Graph of σ^o and σ^{oo} vs θ_s for a Lossy Dielectric, $\theta_i = 30^o$, Large Slope, Small Cell.

Figure 7. Graph of σ^{o} and σ^{oo} vs θ_{s} for a Perfect Conductor, $\theta_{i} = 30^{\circ}$, Large Slope, Intermediate Cell.

Figure 8. Graph of σ^o and σ^{oo} vs θ_s for a Lossy Dielectric, $\theta_i = 30^o$, Large Slope, Intermediate Cell.

Figure 9. Graph of σ° and $\sigma^{\circ\circ}$ vs θ_s for a Perfect Conductor. $\theta_1 = 75^\circ$, Small Slope,Small Cell.
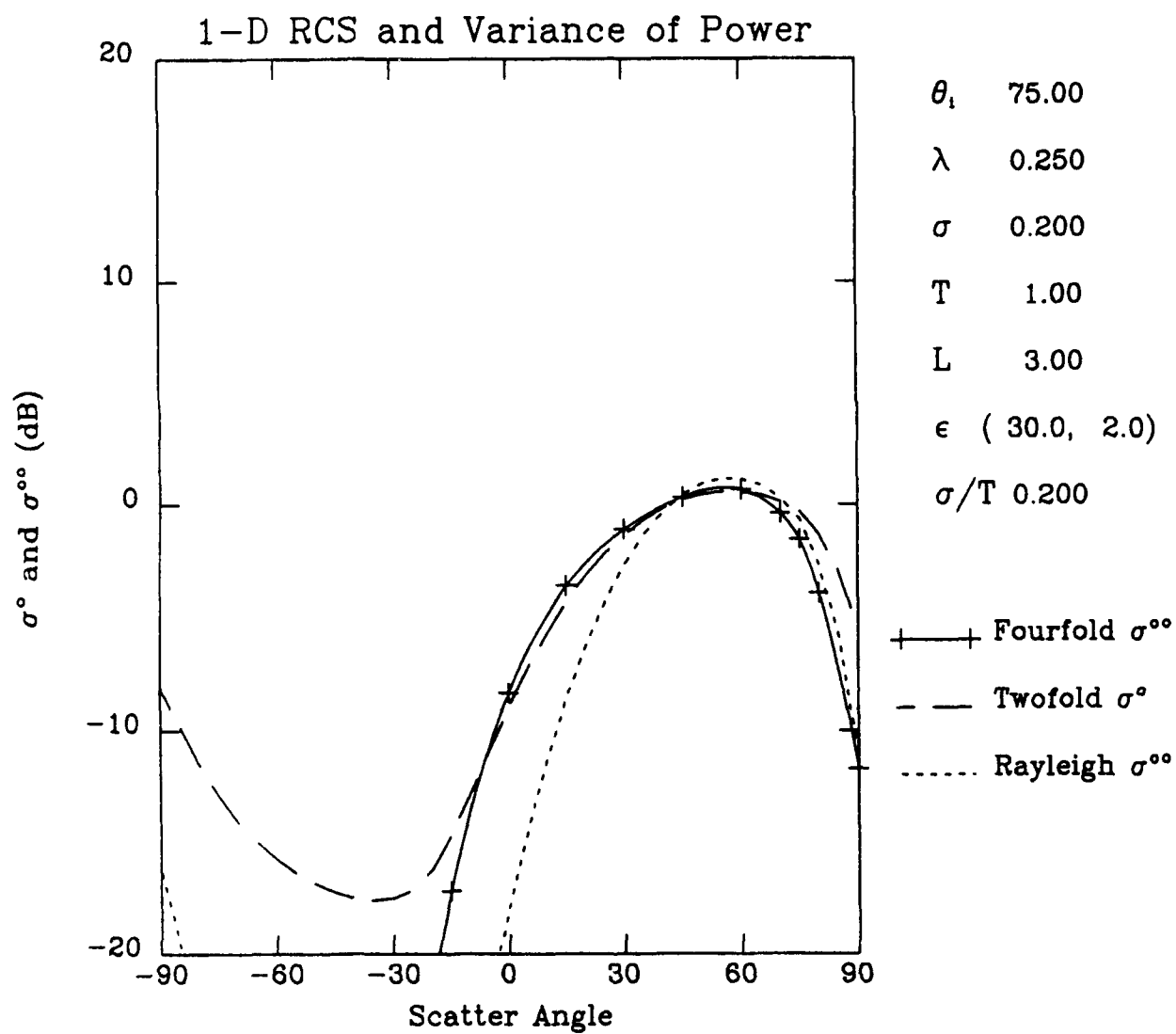
Figure 10. Graph of σ^o and σ^{oo} vs θ_s for a Lossy Dielectric, $\theta_i = 75^o$, Small Slope, small Cell.
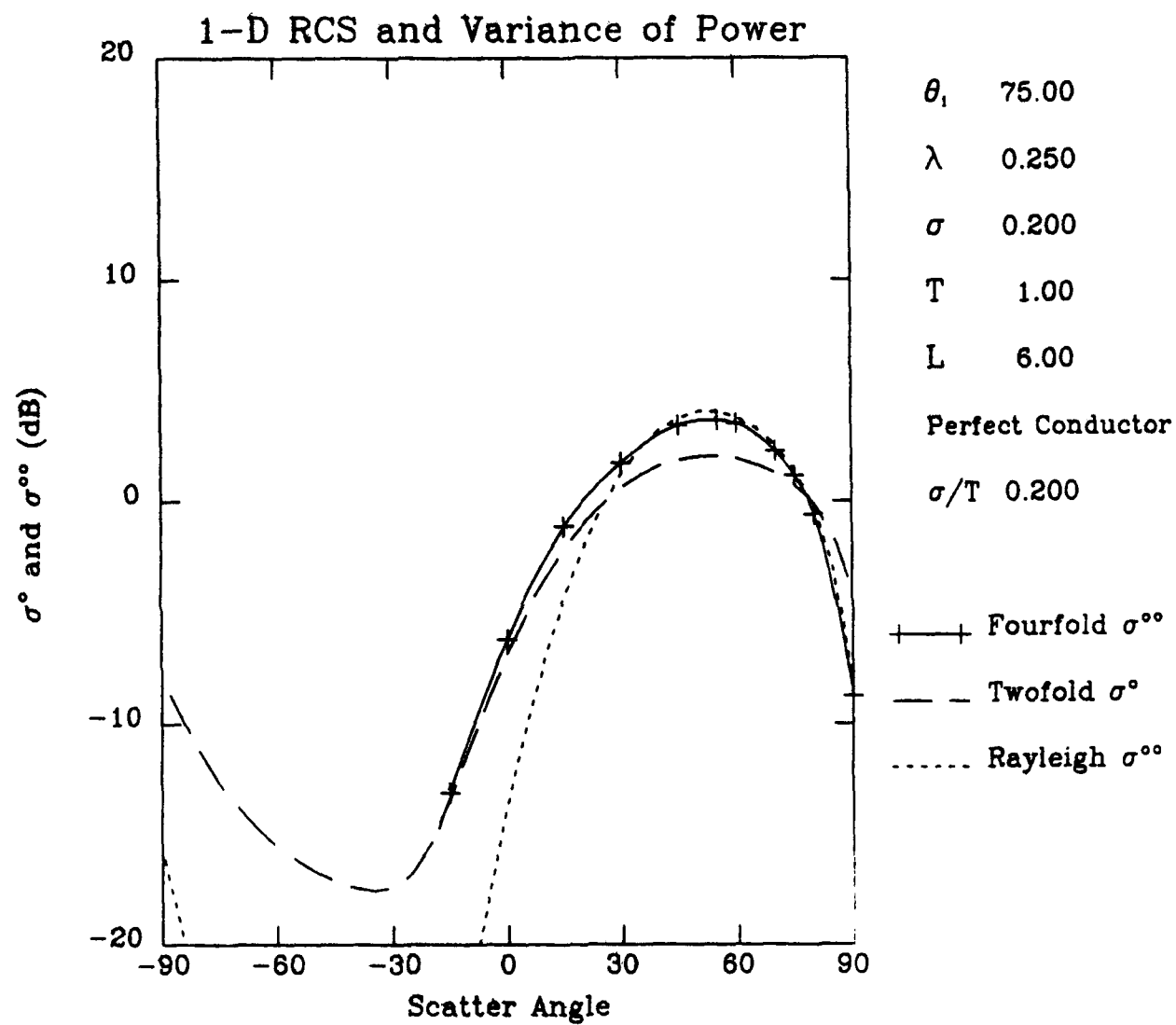
1-D RCS and Variance of Power

θ_i 75.00

λ 0.250

σ 0.200

T   1.00

L   6.00

Perfect Conductor

σ/T 0.200

—┼— Fourfold σ^{oo}

— — Twofold σ^o

...... Rayleigh σ^{oo}

Figure 11. Graph of σ^o and σ^{oo} vs θ_s for a Perfect Conductor, $\theta_i = 75°$, Small Slope, Intermediate Cell.
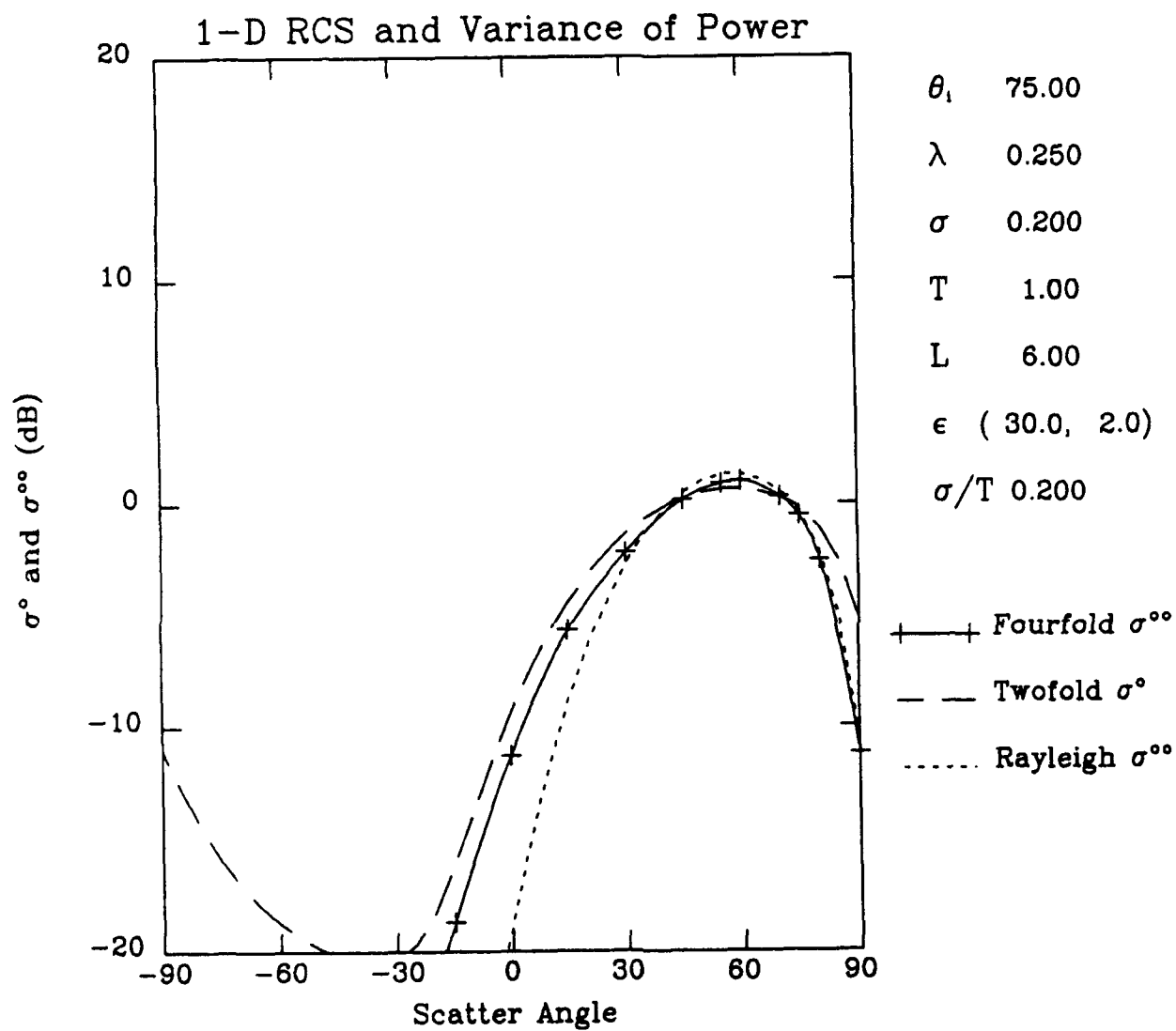
Figure 12. Graph of σ^o and σ^{oo} vs θ_s for a Lossy Dielectric, $\theta_i = 75^\circ$, Small Slope, Intermediate Cell.
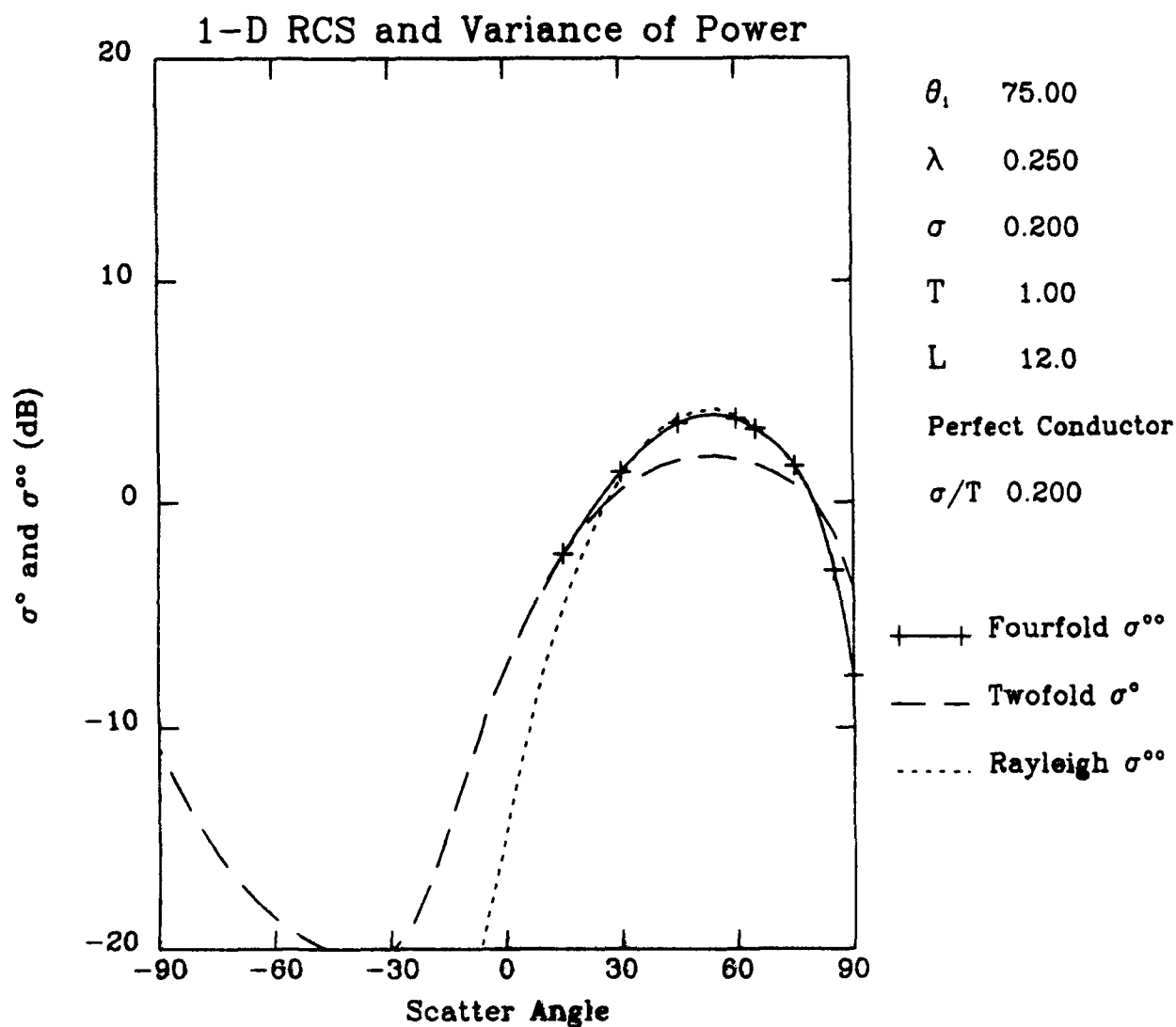
Figure 13. Graph of σ° and $\sigma^{\circ\circ}$ vs θ_s for a Perfect Conductor, $\theta_i = 75^\circ$, Small Slope, Large Cell.
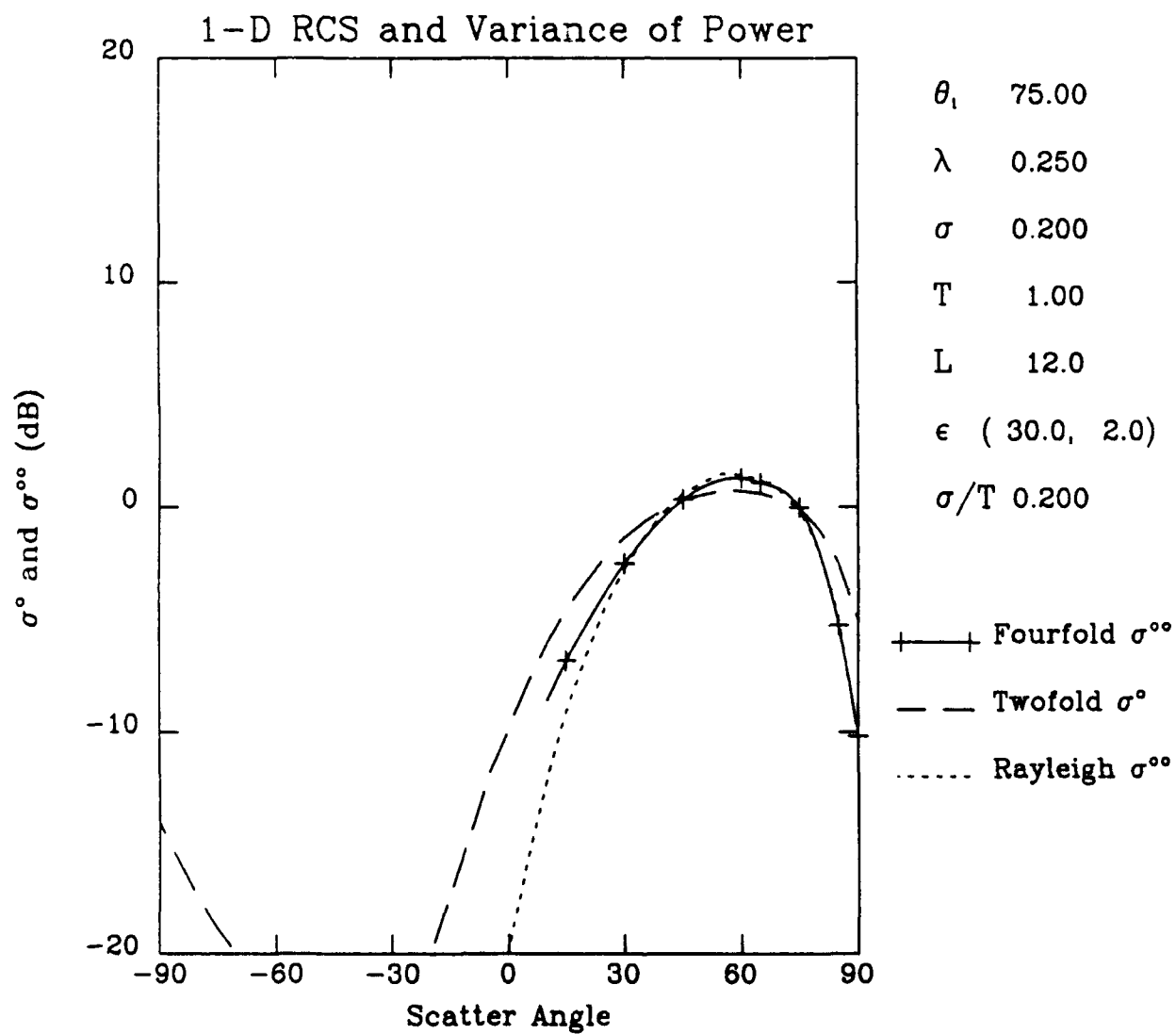
Figure 14. Graph of σ^o and σ^{oo} vs θ_s for a Lossy Dielectric, $\theta_i = 75^o$, Small Slope, Large Cell.
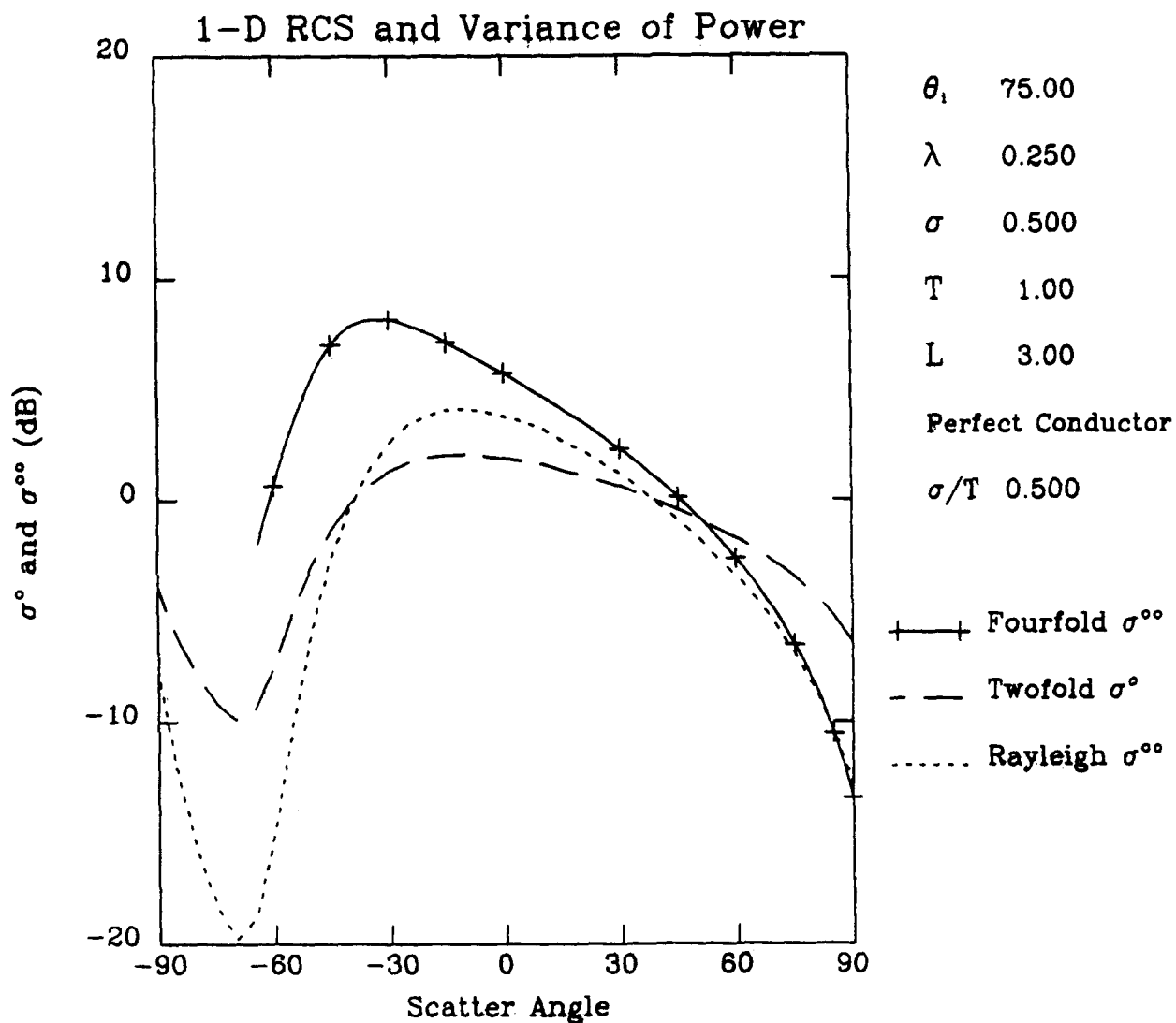
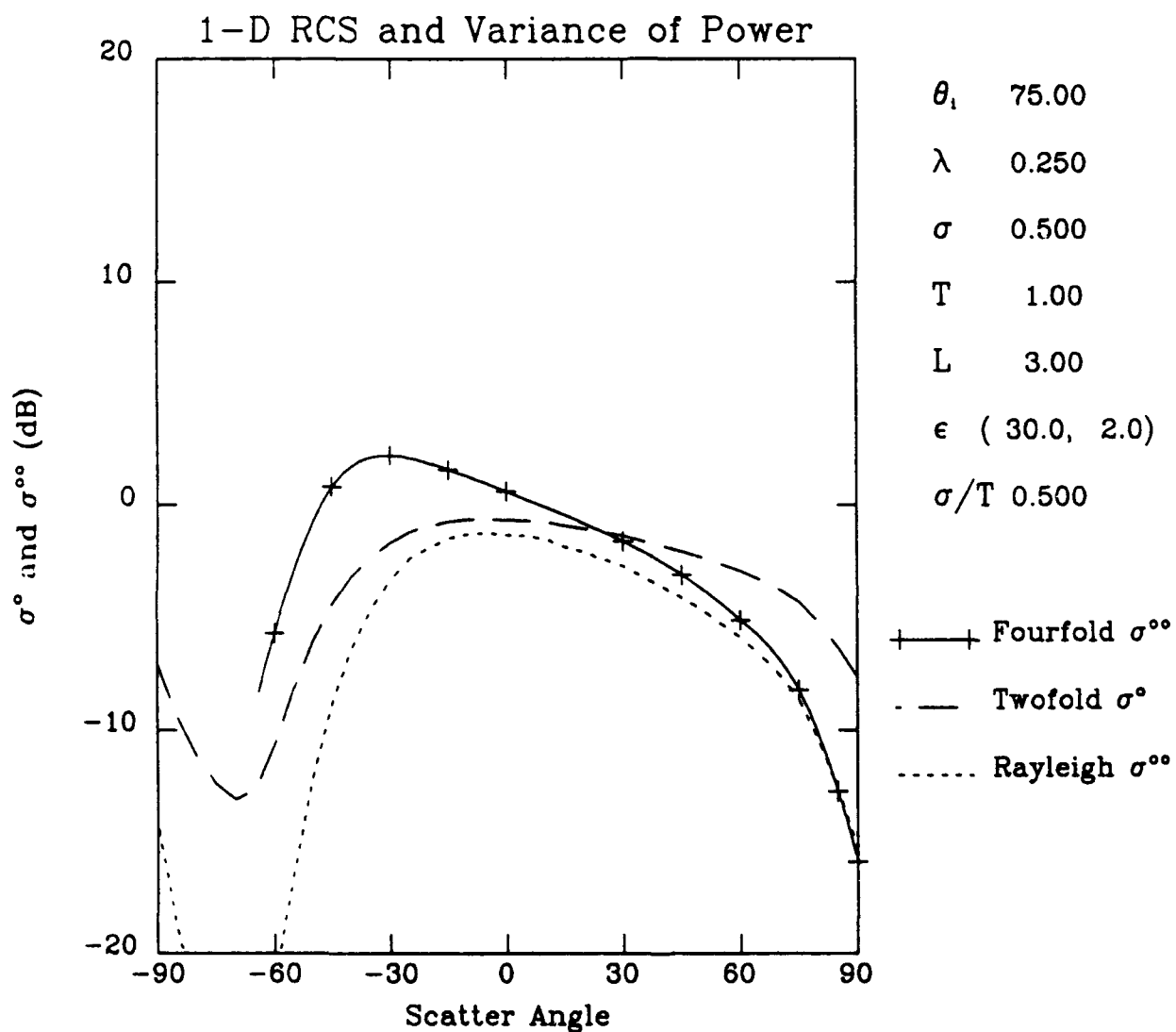**Figure 15. Graph of σ⁰ and σᵒᵒ vs θ_s for a Perfect Conductor. θ_i = 75°, Large Slope, Small Cell.**

Figure 16. Graph of σ^{o} and σ^{oo} vs θ_s for a Lossy Dielectric, $\theta_i = 75^{o}$, Large Slope, Small Cell.
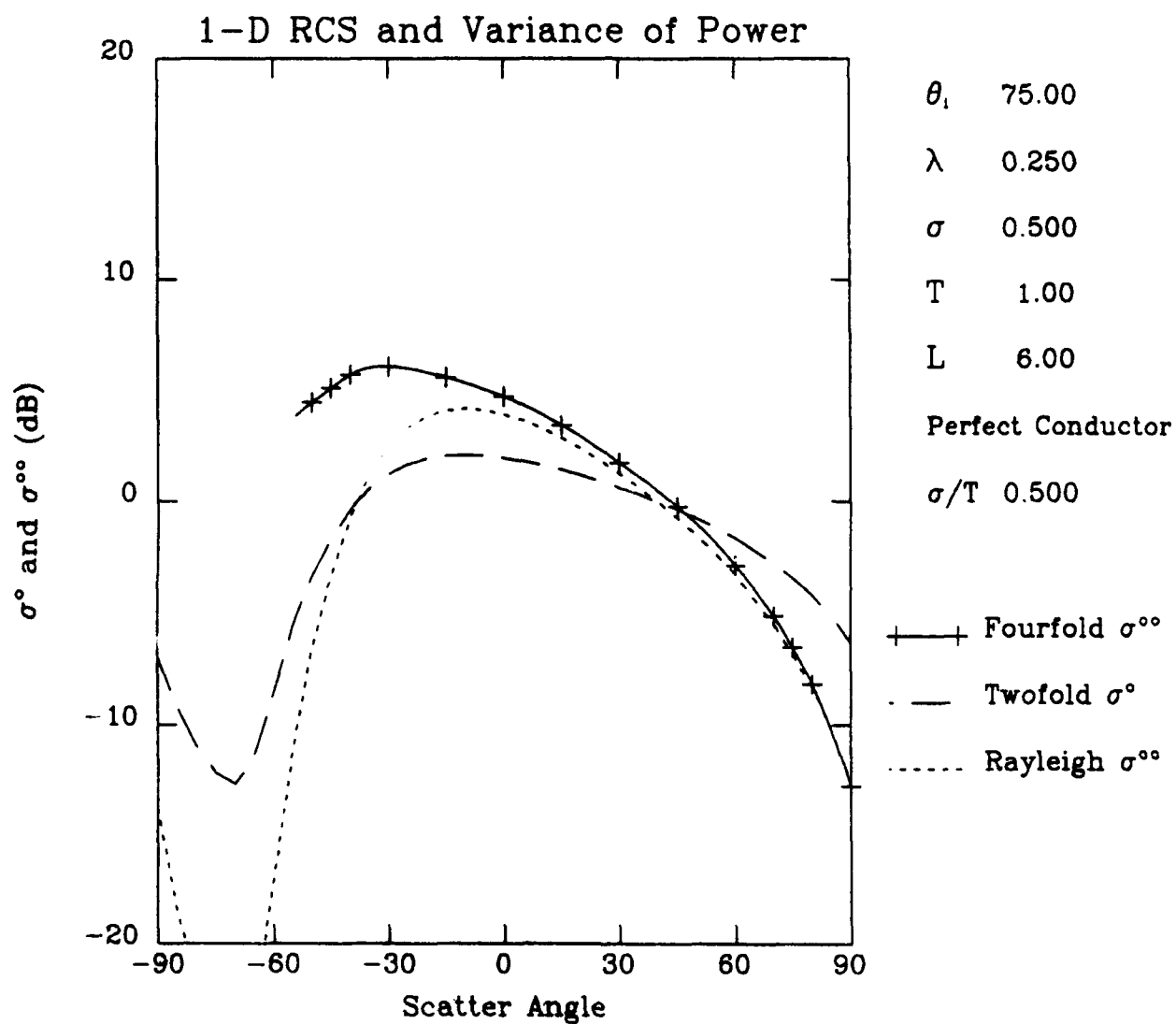
Figure 17. Graph of σ^o and σ^{oo} vs θ_s for a Perfect Conductor, $\theta_i = 75^o$, Large Slope, Intermediate Cell.

1-D RCS and Variance of Power

θ_i 75.00

λ 0.250

σ 0.500

T 1.00

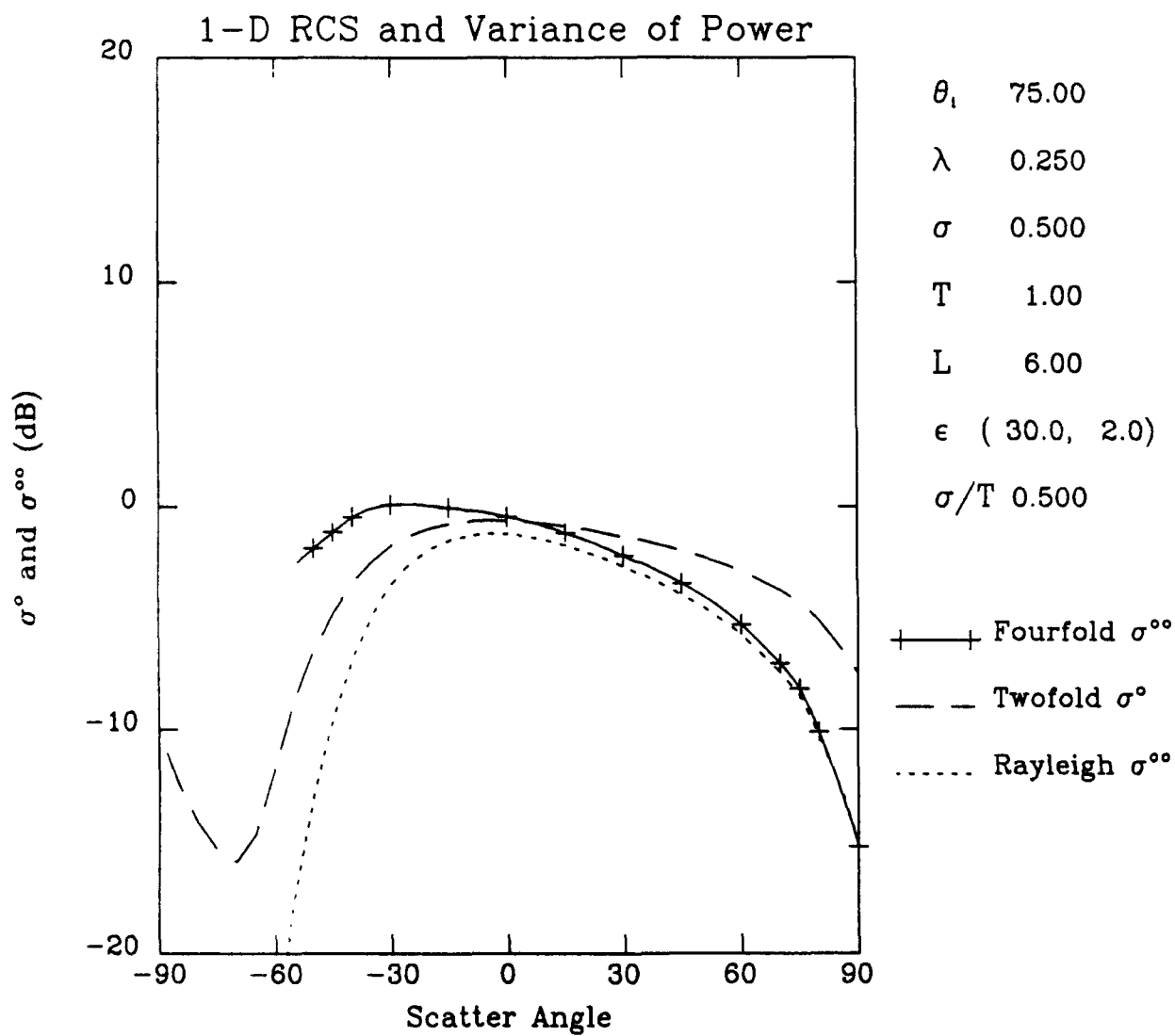L 6.00

ϵ (30.0,   2.0)

σ/T 0.500

Figure 18. Graph of σ^o and σ^{oo} vs θ_s for a Lossy Dielectric, $\theta_i = 75^o$, Large Slope, Intermediate Cell.

Figure 19. Graph of σ^o and σ^{oo} vs θ_s for a Perfect Conductor, $\theta_i = 30^o$, Small Slope, Small Cell, S-Band.

Figure 20. Graph of σ^o and σ^{oo} vs θ_s for a Lossy Dielectric, $\theta_i = 30^\circ$, Small Slope, Small Cell, S-Band.
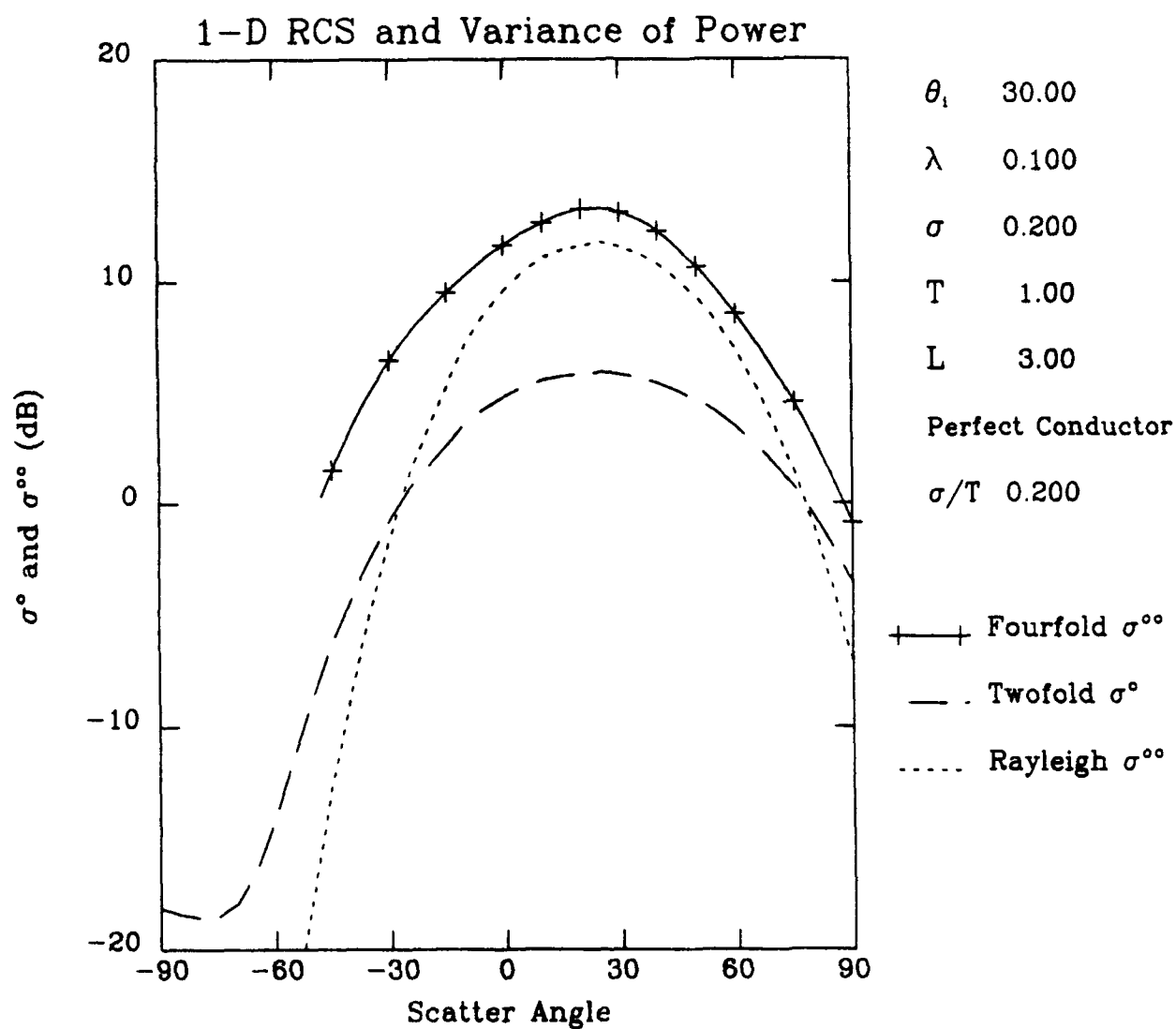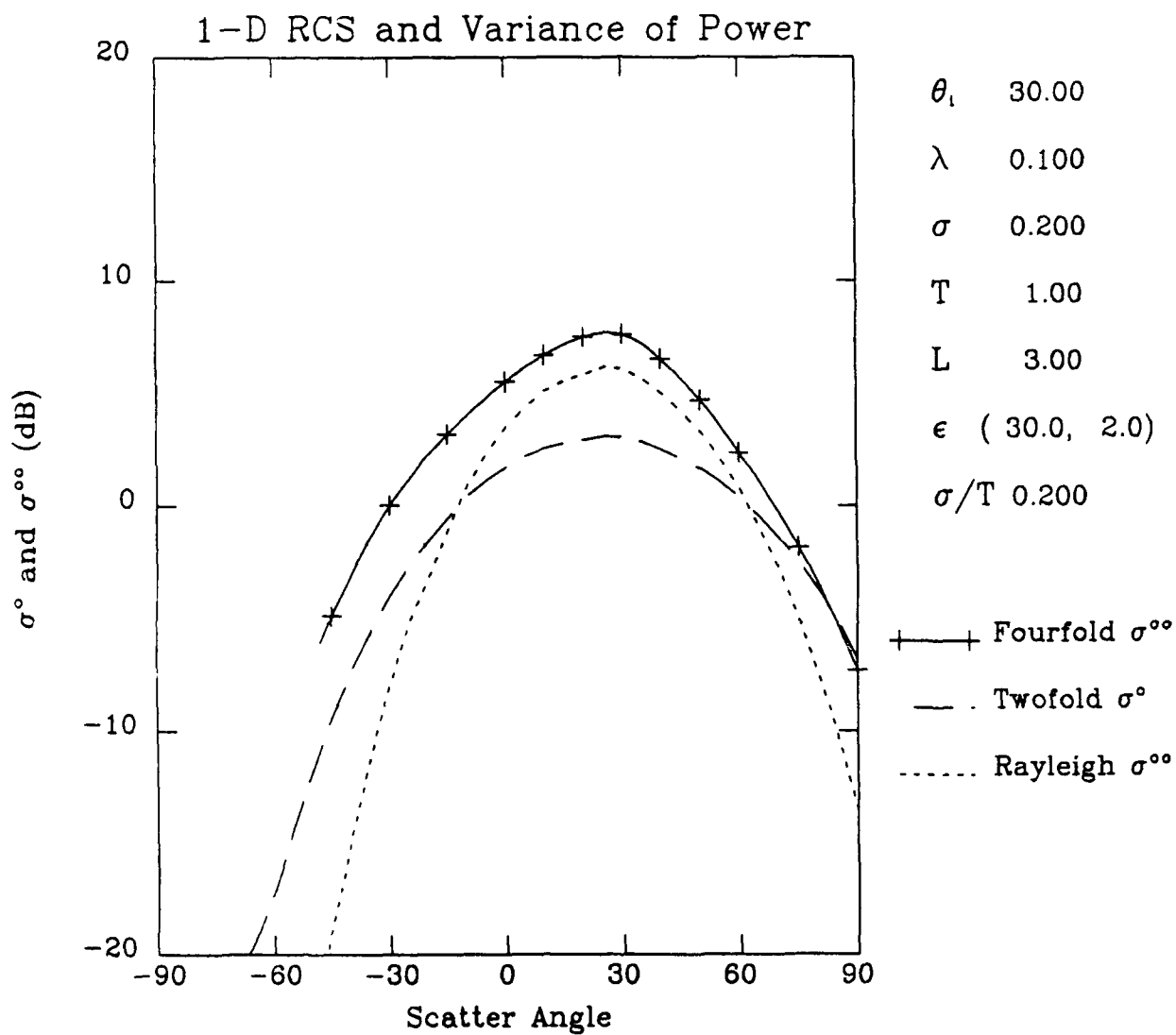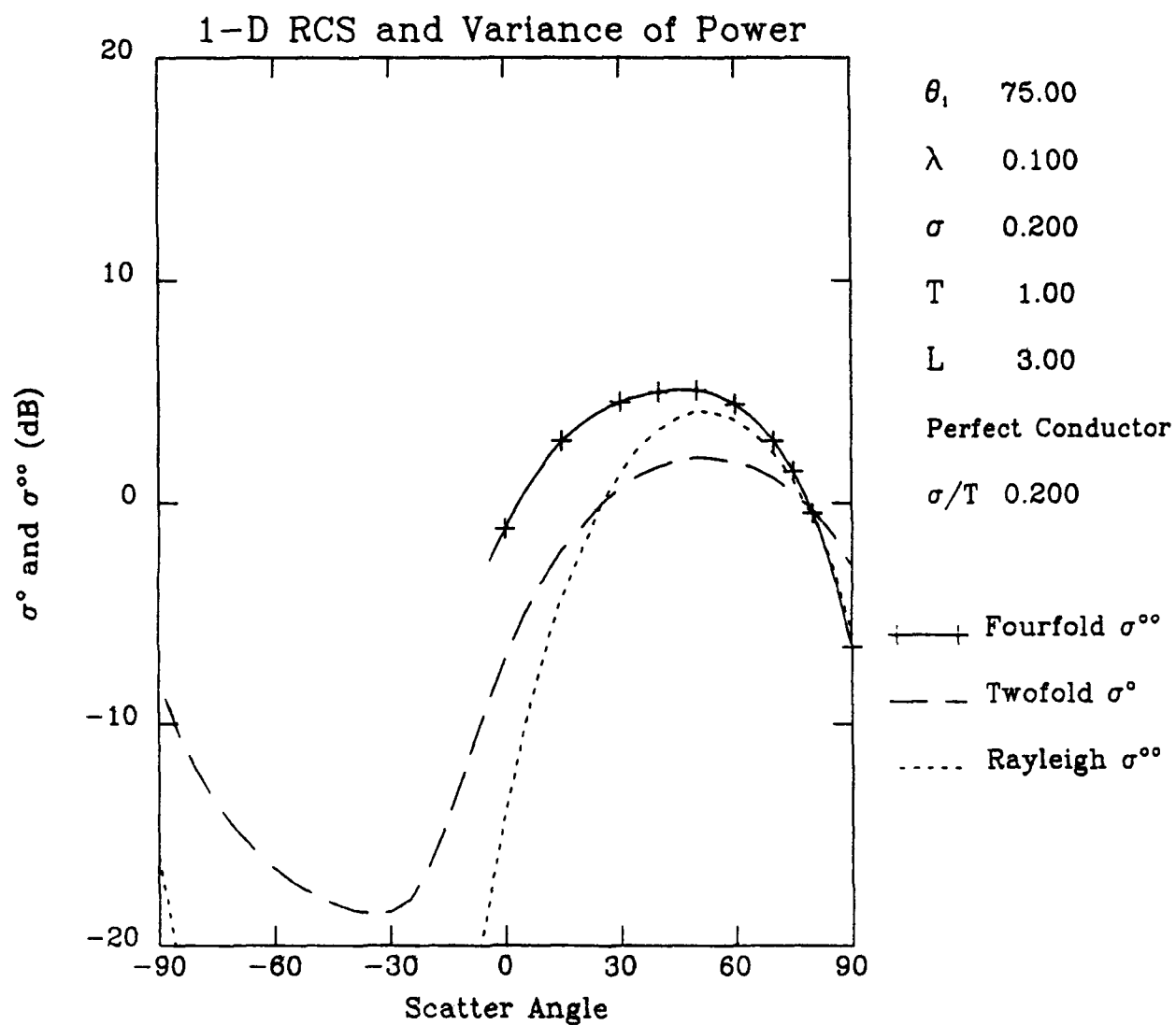
Figure 21. Graph of σ^o and σ^{oo} vs θ_s for a Perfect Conductor, $\theta_i = 75^o$, Small Slope, Small Cell, S-Band.

Figure 22. Graph of σ° and $\sigma^{\circ\circ}$ vs θ_{s} for a Lossy Dielectric, θ_{i} = 75°, Small Slope, Small Cell, S-Band.

1-D RCS and Variance of Power

θ_1 75.00

λ 0.100

σ 0.200

T   1.00

L   6.00

Perfect Conductor

σ/T 0.200

+——+ Fourfold σ^{oo}

— — Twofold σ^o

······· Rayleigh σ^{oo}

σ^o and σ^{oo} (dB)

Scatter Angle

Figure 23. Graph of σ^o and σ^{oo} vs θ_s for a Perfect Conductor, θ_1 = 75°, Small Slope, Intermediate Cell, S-Band.
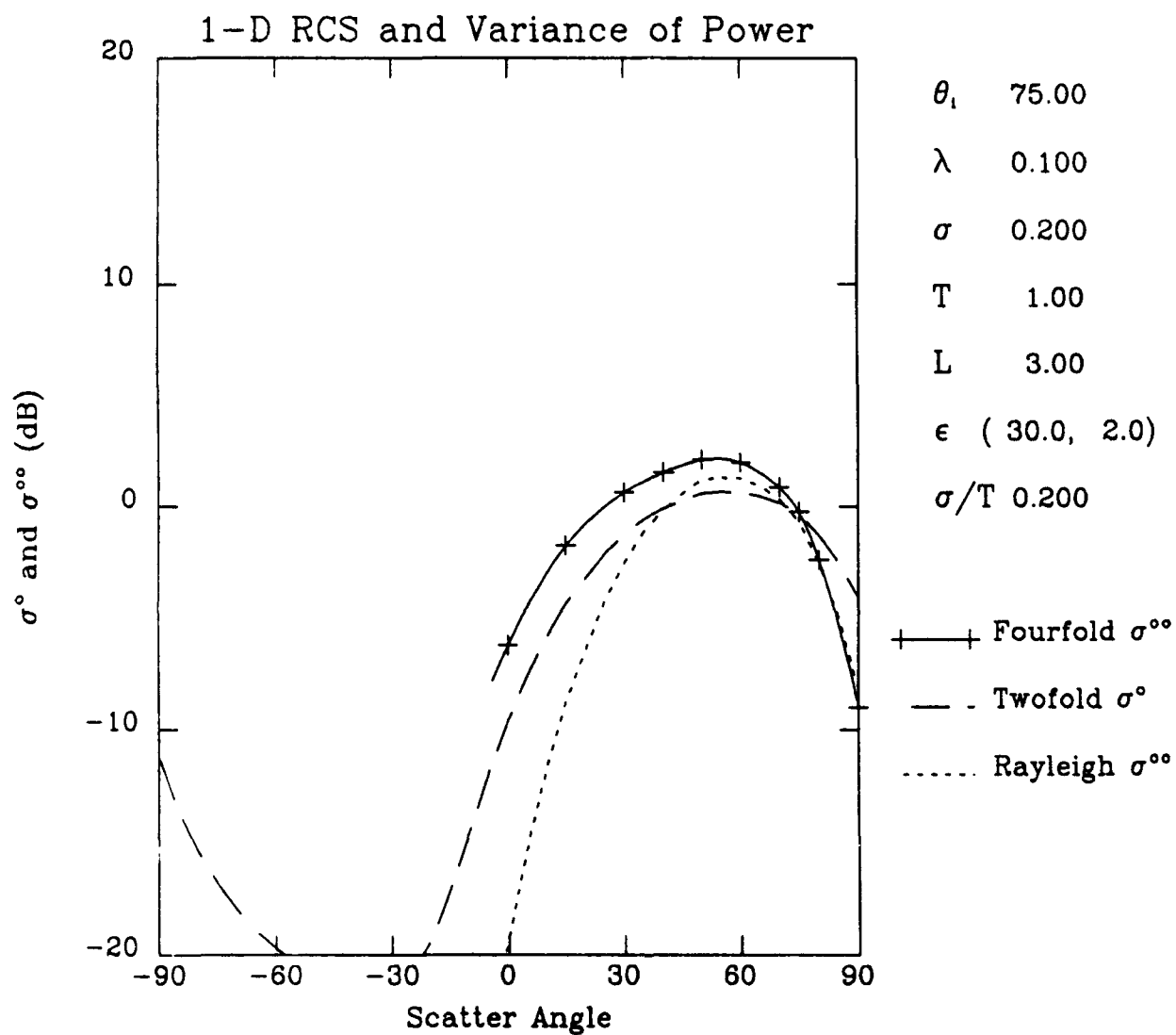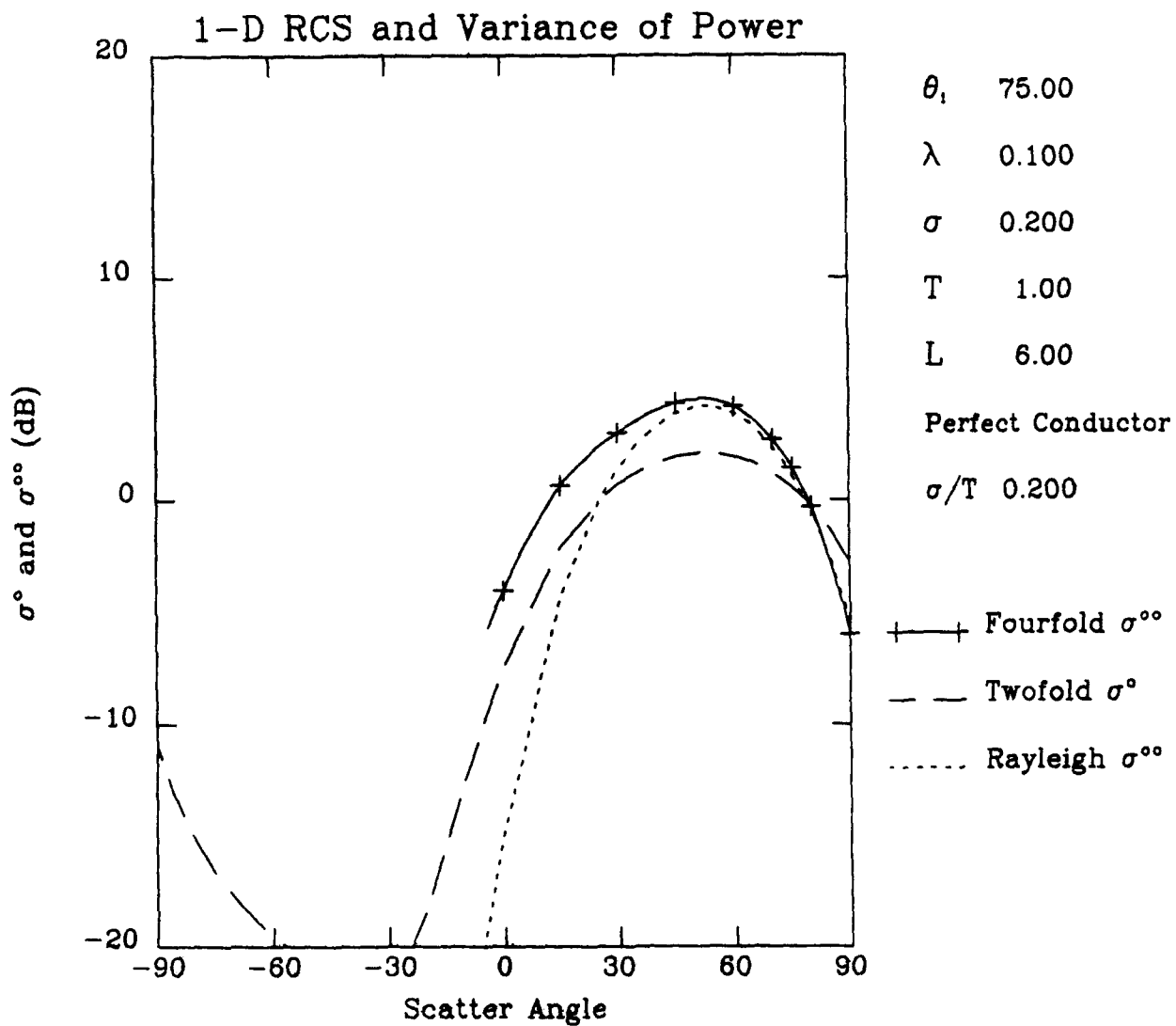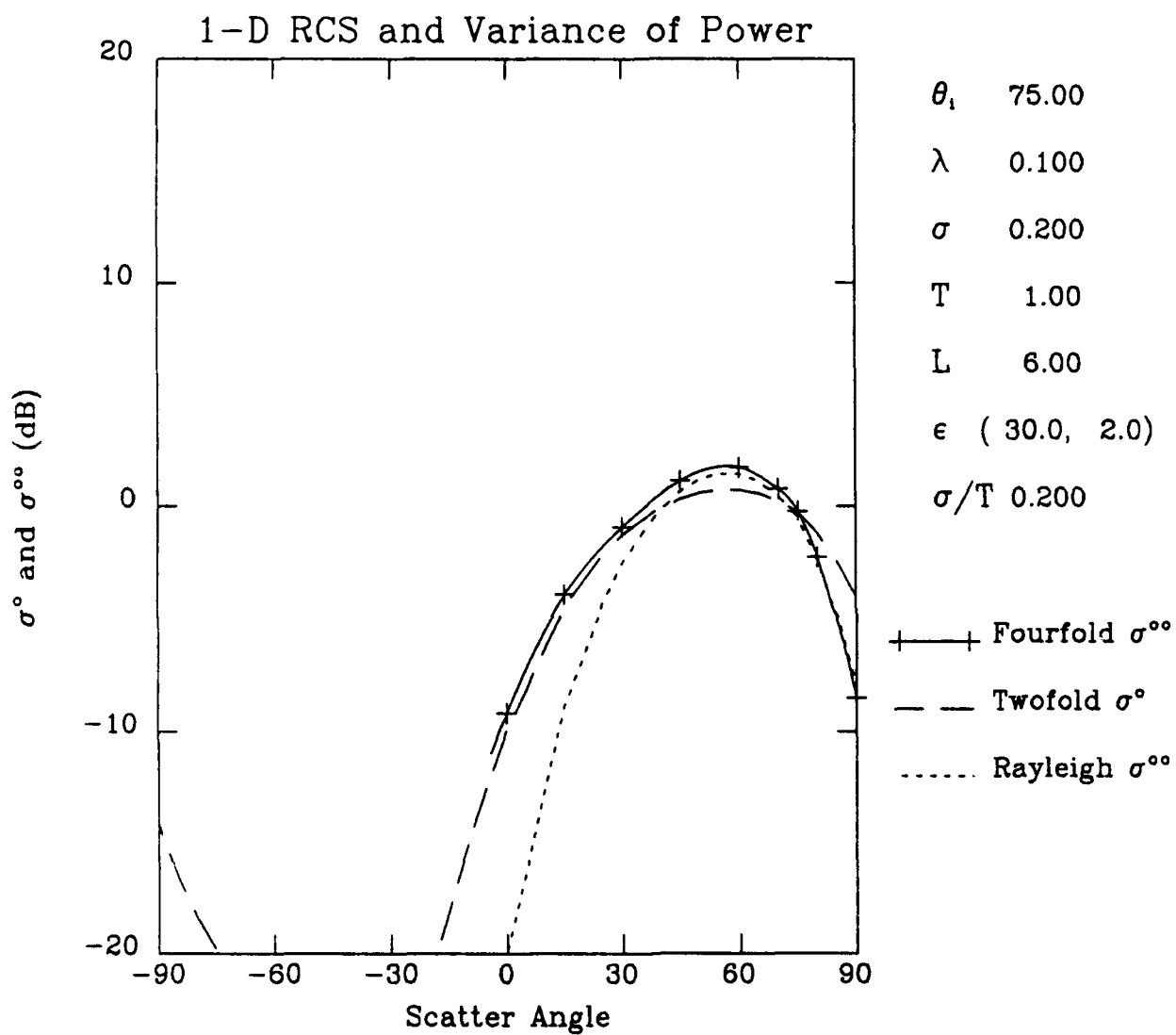
Figure 24. Graph of σ^o and σ^{oo} vs θ_s for a Lossy Conductor, $\theta_i = 75^o$, Small Slope, Intermediate Cell, S-Band.

5.   SUMMARY AND CONCLUSIONS

Reviewing Figures 1 through 24, some general statements about the behavior of σ^{oo} and σ^o may be made. First, for our definitions, $\sigma^{oo} = (\sigma^o)^2$ for a Rayleigh distribution. The normalized variance σ^{oo} is always less than the mean cross section σ^o. The normalized variance σ^{oo} and the mean cross section σ^o both decrease as the angle of incidence θ_i increases, with all other parameters fixed. The normalized variance σ^{oo} becomes close to Rayleigh scatter as the cell size L increases. In the specular direction, σ^{oo} is very close to the Rayleigh value of $(\sigma^o)^2$. The mean normalized cross section σ^o decreases as the cell size increases only for the backscatter region $(\theta_s < 0^o)$. Both σ^{oo} and σ^o are smaller in magnitude for a lossy dielectric than for a perfect conductor.

There are several factors controlling the distribution of the scattered power: (1) The diffuse power scattered in the region inside of an angular band surrounding the specular direction tends to be Rayleigh for cell sizes $L \geq 3T$. (2) When the cell size $L \leq 6T$, the distribution of scattered power is non-Rayleigh outside of an angular region surrounding the specular direction, $\theta_i + 30^o < \theta_s < \theta_i - 30^o$. (3) For a fixed cell size L, the distribution becomes less Rayleigh as the scattering angle θ_s moved away from the angular band surrounding the specular direction, and the departure from the Rayleigh distribution is more pronounced in the backscatter direction $\theta_s < 0^o$, compared to the forward scatter direction.

These trends are true for both a perfect conductor and a lossy dielectric. Also, these trends are true at both L-band and S-band frequencies. Increasing the frequency from L-band to S-band causes the distribution of the scattered power to become more non-Rayleigh.

Finally, it may be noted that increasing the surface roughness tends to make the distribution of the scattered power more non-Rayleigh. This increase in surface roughness may be due to either an increase in the standard deviation of surface height σ or a decrease in the wavelength λ. Increasing the surface roughness tends to make the diffuse scattered power more spatially isotropic, in general. Also, the angular width of the region in θ_s about the specular direction where σ^o has significant magnitude decreases as the angle of incidence θ_i increases.

The distribution in scattered power tends to be more Rayleigh in and near the specular direction, because there are more facets which can contribute to scattering in this direction. There is a Gaussian distribution in the slopes of the facets, and the maximum of this distribution of slopes lies precisely in the specular direction. There are relatively few facets with appropriate slopes in the backscatter direction $(\theta_s < 0^o)$, so that the departure from the Rayleigh distribution is large for the scattered power.

References

1. Papa, R.J., and Woodworth, M. (1988) *The Numerical Evaluation of a Physics Optics Normalized Cross Section for a Rough Surface*, RADC-TR-87-280, ADA198919.

2. Beckmann, P., and Spizzichino, A. (1987) *The Scattering of Electromagnetic Waves from Rough Surfaces*, Artech House, Inc., Dedham, MA.

3. Stark, H., and Woods, J. (1986) *Probability, Random Processes and Estimation Theory for Engineers*, Prentice-Hall, New York.

4. Press, W.H., and Farrar, G.R. (1990) Recursive stratified sampling for multidimensional Monte Carlo integration, *Computers in Physics*, 4:190-195, March/April.

5. Press, W.H., and Teukolsky, S.A. (1989) Quasi- (that is, sub-) random numbers, *Computers in Physics*, 3:76-79, November/December.

6. Shampine, L.F., and Allen, R.C. (1973) *Numerical Computing: An Introduction*, W.B. Saunders Company.

MISSION

OF

ROME LABORATORY

Rome Laboratory plans and executes an interdisciplinary program in re-search, development, test, and technology transition in support of Air Force Command, Control, Communications and Intelligence (C^3I) activities for all Air Force platforms. It also executes selected acquisition programs in several areas of expertise. Technical and engineering support within areas of competence is provided to ESD Program Offices (POs) and other ESD elements to perform effective acquisition of C^3I systems. In addition, Rome Laboratory's technology supports other AFSC Product Divisions, the Air Force user community, and other DOD and non-DOD agencies. Rome Laboratory maintains technical competence and research programs in areas including, but not limited to, communications, command and control, battle management, intelligence information processing, computational sciences and software producibility, wide area surveillance/sensors, signal proces-sing, solid state sciences, photonics, electromagnetic technology, super-conductivity, and electronic reliability/maintainability and testability.